Design, Fabrication, and Characterization of a Motion Stage for Scalable Imprinting of DNA Nanowires

by

John J. LaColla

Submitted to the
Department of Mechanical Engineering
in Partial Fulfillment of the Requirements for the Degree of

Bachelor of Science in Mechanical Engineering

at the

MASSACHUSETTS INSTITUTE OF TECHNOLOGY

ARCHIVES

MASSACHUSETTS INSTITUTE OF TECHNOLOGY
JUN 28 2012
LIBRARIES

June 2012

© 2012 Massachusetts Institute of Technology
All rights reserved.

Signature of Author.....
Department of Mechanical Engineering
May 22, 2012

Certified by.....
Martin L. Culpepper
Associate Professor
Thesis Supervisor

Accepted by.....
John H. Lienhard V
Collins Professor of Mechanical Engineering
Chairman, Undergraduate Thesis Committee

Design, Fabrication, and Characterization of a Motion Stage for Scalable Imprinting of DNA Nanowires

by

John J. LaColla

Submitted to the Department of Mechanical Engineering
on May 22, 2012 in Partial Fulfillment of the
Requirements for the Degree of

Bachelor of Science in Mechanical Engineering

ABSTRACT

This thesis work examines the scalability of an imprinting stage utilizing parallel self-aligning mechanisms in a DNA combing and imprinting (DCI) process. Scalability is vital in developing efficient, low-cost and high-yield manufacturing processes, and improving the scalability of the DCI imprinting process will benefit biomedical research by enabling the affordable and scalable production of micro/nanoarrays for drug discovery, protein isolation, nanofluidics, and other applications. Previous work on the DCI process has primarily focused on the mechanics of the imprinting process rather than scale, and misalignments between the stamp and slide surfaces make it difficult to increase the scale without drastically increasing the complexity of the system, particularly when a 3 degree of freedom positioning device is used.

Herein, a 1 degree of motion stage with 3 independent, passive self-aligning mechanisms is demonstrated to achieve high performance at 3 times the scale of previous devices. The influence of kinematic coupling repeatability, parallelism, and linear motion parasitics on the performance of the imprinting device was identified, and the device's performance was measured. The repeatability of the kinematic couplings and the magnitude of the parasitic motions were found to exceed the gage resolution of 12.7 μm, and the initial parallelism variation of the stage is less than 140 μm.

A mathematical model to quantify the scalability of the device was also developed by examining its ability to handle misalignments in the stage, stamp, and slide alignment. Analysis with the model demonstrated the ability of the device to accommodate maximum misalignments ranging from 3.9° to 9.3°, confirming the minimal performance-scale tradeoff of a 1 degree of freedom motion stage. Through this analysis, this thesis demonstrates the effectiveness of parallel, self-aligning stamp mechanisms in a scalable DCI process, and provides a framework for future development of scalable imprinting stages.

Thesis Supervisor: Martin L. Culpepper
Title: Associate Professor

ACKNOWLEDGEMENTS

First, I would like to thank Sourabh Saha for his support and guidance throughout my UROP and thesis work. His experience and resourcefulness were pivotal in my completion of this project.

I would also like to thank Professor Martin Culpepper for the opportunity to work in the Precision Compliant Systems Lab this year.

I'd also like to thank MIT and the Department of Mechanical Engineering for the incredible undergraduate experience. Thank you for all the knowledge, opportunities, support, memories, and late nights. I wish all of my fellow students the best of luck in the future.

I owe a large part of my success to the continued support of my family and friends. Thank you all for your unending support, and for pushing me to become who I am today.

CONTENTS

FIGURES

TABLES

CHAPTER 1

INTRODUCTION

The purpose of this thesis work is to (i) design and fabricate a self-aligning imprinting stage and (ii) examine the scalability of the stage in terms of scale and quality of production. In order to quantify scalability, it is necessary to (i) identify factors that quantify the scalability of the apparatus, (ii) examine the factors that influence these metrics and (iii) link these metrics to the imprinting stage's performance. By developing measurable metrics for scalability, it will be possible to examine the effectiveness of the self-aligning imprinting stage design. Analysis of the apparatus' performance will allow for the identification of potential limitations and flaws in the current design of the stage, and will serve as guidelines for revision and future development of such equipment.

Scalability of equipment is a key factor in efficient manufacturing processes. It is important that the factors affecting scalability be known, so that not only are the limitations of a particular device or process known, but potential improvements can also be identified. This equipment will be used to imprint DNA nanowires to make micro-scale chips. These chips must be manufactured in large quantities, at low cost, and at a high rate for maximum benefit. Consequently, for this device, scalability is defined as the ability to produce multiple chips with minimal adjustment to the structure of the device. These chips will be used in biomedical research and similar applications, and characterizing the performance metrics of this device will support such research by making micro/nanoarray chips more readily available to researchers.

While the effectiveness of a single self-aligning device for DCI imprinting has been shown in previous work, such a setup is not scalable. Other alignment schemes utilizing 3 degrees of motion provide quality results, but are not scalable due to the complexity of such a system. To a large degree, this is because previous efforts have focused primarily on the mechanics of the imprinting process, rather than on the quantification and implementation of scalable design metrics. Here, a scalable device for DCI imprinting is demonstrated to utilize self-alignment to reduce the required degrees of motion to 1. Further, the design factors of this device that influence scalability have been defined and examined, demonstrating the scalable nature of the device. In particular, this device, shown in Figure 1.1 increases the output of the imprinting process by a factor of 3, while maintaining the high performance necessary for high quality chips.

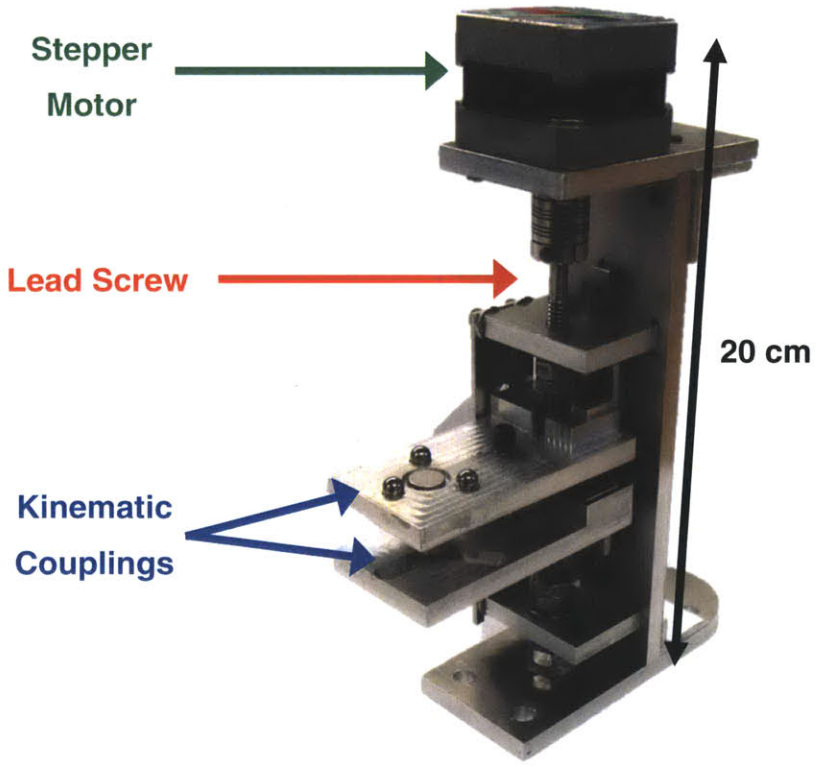

Figure 1.1: Photograph of imprinting stage.

The theory and justification for the scalability metrics are discussed in Chapter 2, with discussion on the importance of kinematic coupling repeatability and predictable stage motion. Chapter 3 introduces the experimental setup for analysis of kinematic coupling repeatability and the characterization of the linear stage motion, and presents the results of the experiments. Presented in Chapter 4 is a discussion of the experimental results, and identifies the design features and considerations that are most important for future work on self-aligning imprinting devices.

1.1 Problem Definition

1.1.1 DCI Imprinting Process Overview

The DNA combing and imprinting (DCI) manufacturing process is used in the manufacturing of nanochannels. DNA nanostrands are attached to a patterned PDMS stamp through a process called combing, when the stamp is drawn through a DNA solution, leaving nanostrands connecting adjacent micropillars on the stamp. The stamp is then gold plated, and inverted against a glass slide for imprinting. A polymer resin is injected around the stamp, forming the nanochannels and microwells, and is cured with UV light. The gold plating is etched away and the stamp is removed, leaving the microwells and nanochannels intact. Figure 1.2 provides an overview of the process.[1]

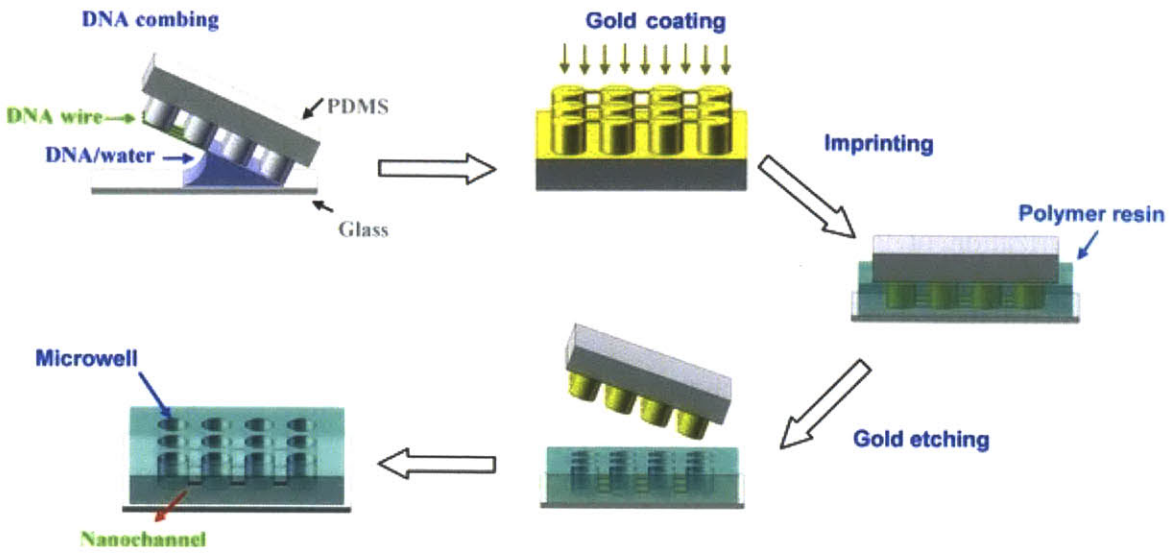

Figure 1.2: Schematic of DCI manufacturing process

One of the biggest concerns with the DCI process is the low yield of the process, which is largely due to the fragility of the stamps and DNA strands. Since they are easily damaged, it is important that they be handled with care to ensure low contact forces and no-slip contact throughout the imprinting process; otherwise the final products will have defects. Handling the stamps directly is difficult, and a stamp holder is typically employed to provide a sturdy surface for operators to handle. In addition, misalignments between the stamp and slide during the imprinting can cause defects and reduce overall yield; this is discussed further in Section 1.1.2.

Finally, in-plane movement is another major concern in the DCI process. Throughout the time that the stamp and slide are making contact, it is crucial that they do not slip along each other. Once the stamp and slide make their initial contact, the remainder of the travel must be as vertical as possible, to minimize the dragging of the stamp along the slide, or vice versa. Friction forces between the two surfaces can damage the delicate DNA strands and reduce the yield of the process. Consequently, it is important that any imprinting scheme minimize this in-plane motion as much as possible.

Table 1.1: Process Specifications for Imprinting Device

Property	Goal
Size of Stamp	$10\ \text{mm} \times 10\ \text{mm} \times 3.25 \pm 0.07\ \text{mm}$
Size of Slide	$22\ \text{mm} \times 22\ \text{mm} \times 0.15 \pm 0.02\ \text{mm}$
Critical Alignment Direction	Out-of-plane
Speed of Contact	$< 1\ \text{mm/s}$
Contact Force	< weight of stamp

1.1.2 Alignment of Stamp and Slide

The most important function of a DNA imprinting apparatus is its ability to achieve consistent, repeatable alignment between the stamp and slide faces. This contact is necessary to produce conformal contact between the stamp and the glass slide, which ensures proper dispensing, distribution, and curing of the polymer solution; all these factors are vital for the production of high quality chips.

Figure 1.3 demonstrates a scenario in which the stamp and slide are misaligned by an angle θ during the imprinting process. As the slide travels to make contact with the stamp, the scenario becomes that shown in Figure 1.4, when the edge of the stamp first contacts the slide. It is important that the stamp be able to properly align with the slide with minimal contact forces, because excessive contact or frictional forces may damage the delicate nanostrands on the stamp. If the stamp is fixed in its location, the slide must be reoriented by the alignment stage for imprinting.

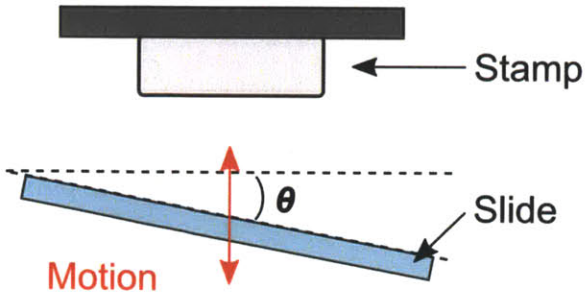

Figure 1.3: Initial position of the stamp and slide. The slide is misaligned by angle θ.

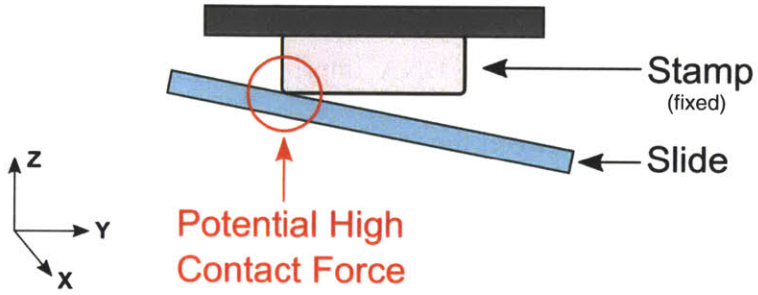

Figure 1.4: Contact between misaligned stamp and slide.

One method for dealing with stamp and slide misalignments involves the use of self-aligning stamp fixtures. This method, depicted in Figure 1.5, relies on the stamp's weight to bring the stamp into contact with the slide The stamp is constrained in two directions (x and y), but is permitted to travel in the z-direction. By allowing the stamp to settle into alignment with the slide under its own weight, the self-alignment technique reduces the risk of high contact forces at the stamp/glass interface. In addition, this 1 degree of freedom passive alignment technique reduces the overall complexity of the system.

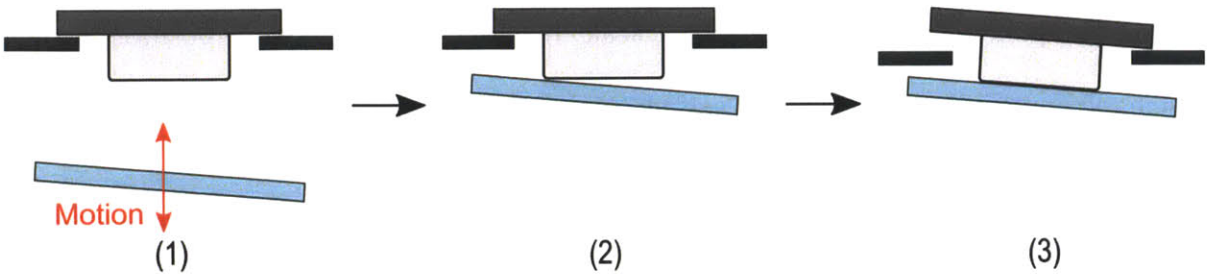

Figure 1.5: The steps involved in self-alignment of the PDMS stamp on a misaligned glass slide.

1.1.3 Device Design Goals

The design of the imprinting apparatus is motivated by the need for a scalable, low-energy imprinting apparatus for DCI manufacturing. The device is aimed for use in a research laboratory setting, and as such, its footprint must be one that fits easily on a lab bench. It is also desirable that the entire DCI manufacturing process be automated in the future, so it is necessary that the device be able to operate as part of a larger system. Table 1.2 presents a summary of the major design goals for the imprinting device described in Chapter 2.

Table 1.2: Design Goals for Imprinting Device

Property	Goal
Automation	Can be incorporated into larger process
Stamp Capacity	> 1
Motion Degrees of Freedom	1
Footprint	< 30 cm $\times$ 30 cm

1.2 Implications of Work

While the concept of self-aligning mechanisms in DCI processes is not unique to this project, this work takes this concept a step further by demonstrating an implementation of self-aligning stamps in a scalable manner. In particular, as described in Section 1.2.1, this work seeks

to improve upon the performance versus scale relationship of a typical positioning device through the implementation of several self-aligning mechanisms in parallel.

1.2.1 Performance vs. Scale

A key aspect of this design process was the need to reduce the tradeoffs between performance and scale of the device. Figure 1.6 demonstrates a typical relationship between performance and scale of a 3 degree-of-freedom positioning device for DNA imprinting. While a 3-dimensional positioning system is well-suited for lower scale applications, such as single stamp imprinting devices, it rapidly becomes less desirable as the scale increases. Adding additional stamps and slides to the system causes it to become complex and costly, as small variations in alignments between each stamp-slide pair make it difficult to accurately position all at once.

Because of the difficulties in implementing a 3 degree-of-freedom system, this work sought to modify the performance-scale relationship in Figure 1.6. The switch to a 1-degree of freedom system results in a system with lower complexity, but requires other design changes to achieve the goal performance-scale curve shown in the figure.

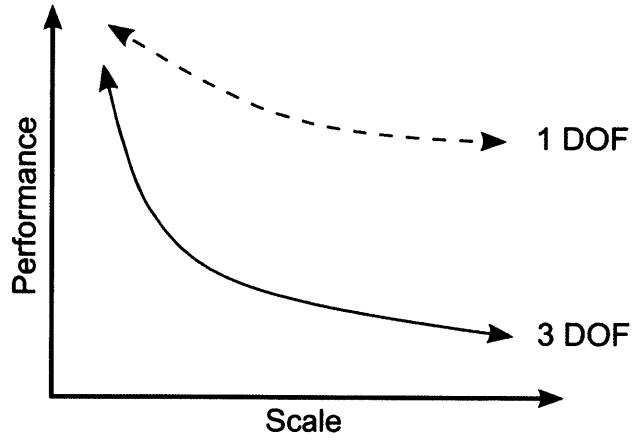

Figure 1.6: Graph of performance versus scale for a typical 3 degree of freedom and the goal relationship for the proposed 1 degree of freedom system.

The introduction of the self-aligning stamps is the major design component that enables this device to achieve the new performance-scale curve. By allowing each stamp to align itself with its slide on an individual basis, the positioning in 2 degrees of freedom is accomplished passively. Small variations in stamp thicknesses, misalignments, and other minor inconsistencies are accommodated by the stamp fixtures themselves, rather than by the entire slide tray.

1.2.2 Relevance of Work to Other Research

This work is particularly beneficial to the biomedical research community, as nano/microwell trays are useful in medical and biological research for protein separation, nanoparticle formation, ion transport, and nanochannel electroporation, among other nanoscale and nanofluidic applications.[1] The introduction of a low-cost, high-performance, scalable, and desktop-sized imprinting device is incredibly desirable, as it enables increased research at a lower cost. In addition, the ability to incorporate the imprinting process with the combing and polymer dispensing processes into a single automated process will enable more researchers to use the device. By simplifying and automating the DCI manufacturing process, the amount of time required to learn to operate the equipment will be greatly reduced, increasing the accessibility of these resources.

CHAPTER

2

DESIGN AND FABRICATION

Based on the design goals and specifications set forth in Chapter 1, an imprinting stage with 1 degree of freedom was designed and built to implement the self-aligning stamp technique described in Section 1.1.2. A CAD model of the device is shown in Figure 2.2, and the design and fabrication is described in this section. Table 2.1 describes the quantitative specifications used to drive the design of the device.

2.1 Overview of Device

The stamps and slides for the DCI imprinting process are loaded into separate trays for handling as a group rather than individual parts. Covers are places onto the trays, and after the combing and gold-plating of the stamps, the trays are loaded into the imprinting stage, where they are aligned with the imprinting stage through kinematic couplings. A magnetic preload holds the trays in place throughout the imprinting process. The stages are attached to a precision linear slide for actuation in the z-direction. A top-mounted stepper motor provides the power to drive a lead screw attached to the linear stages. The lower slide tray is driven upwards to meet with the stamp tray, and the stamps are brought into contact with the slides. A contact switch stops the tray motion at the desired height, and waits for the polymer to be dispensed. A UV light source underneath the slide trays is activated, and the polymer is cured. The stages are then

separated, and the gold plating is etched away, leaving the completed microwell chips behind. Figure 2.1 shows a CAD mockup of the imprinting device, dispensing stage, and UV source.

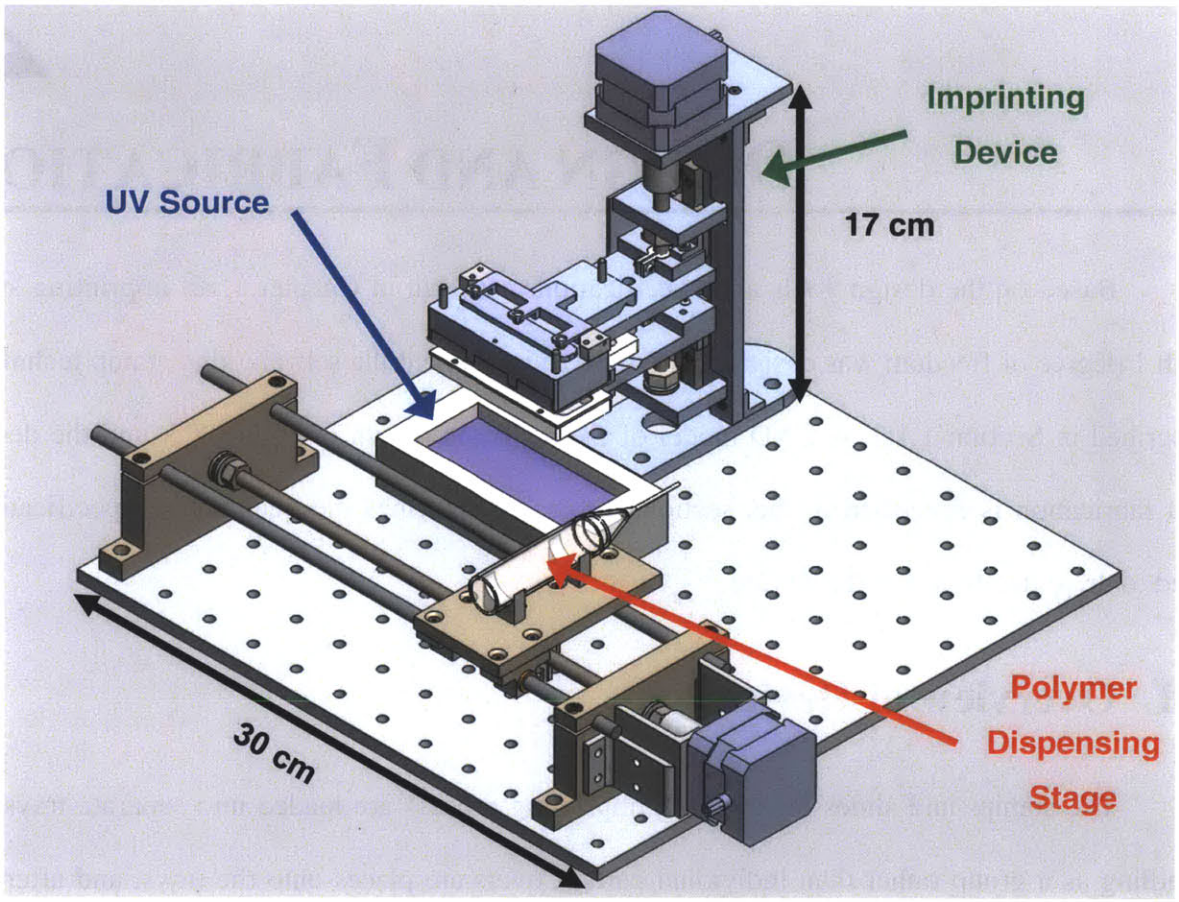

Figure 2.1: CAD drawing showing the position of the imprinting stage with respect to the UV source and dispensing stage.

The imprinting device is constructed primarily of custom fabricated aluminum parts. Leading up from the base of the device is an aluminum backbone, to which the precision linear slide and bearing holders are attached. Rigidity and alignment are provided by a pair of aluminum angle brackets, which connect the vertical beam to the base and the top-mounted stepper motor. A miniature precision rail is attached to the aluminum spine, and provides constraint and guidance for the system's single degree of motion.

A stepper motor is mounted on top of the device, and is coupled to a threaded steel rod to create a lead screw for driving the linear motion of the stage. Moveable stages are coupled to the precision rail through bearing blocks, and utilize through-holes to accommodate the lead screw. Each moveable stage may be fixed in place using a bracket mounted on the side of the device, and similarly, may be configured to engage the lead screw for linear actuation. The stages feature ball-and-groove kinematic couplings with a magnetic preload for the addition and removal of modular trays.

Stamp and slide trays interface with the kinematic couplings on the stages for alignment during the imprinting process. These trays hold either the PDMS stamps or glass slides used in the DCI imprinting process, so that they do not need to be loaded directly into the imprinting device. Rather, the trays may be prepared separately from the imprinting stage, allowing for a reduction of downtime in between imprinting processes.

Table 2.1: Design Specifications for Imprinting Device

Property	Specification
Stamp Capacity	3
Vertical Travel	$5 - 15$ mm
Height	~ 105 mm
Footprint	< 30 cm $\times$ 30 cm
Maximum Stamp Tray Weight	0.5 kg
Maximum Misalignment Handled	In-plane: N/A Out-of-plane: $> 3°$

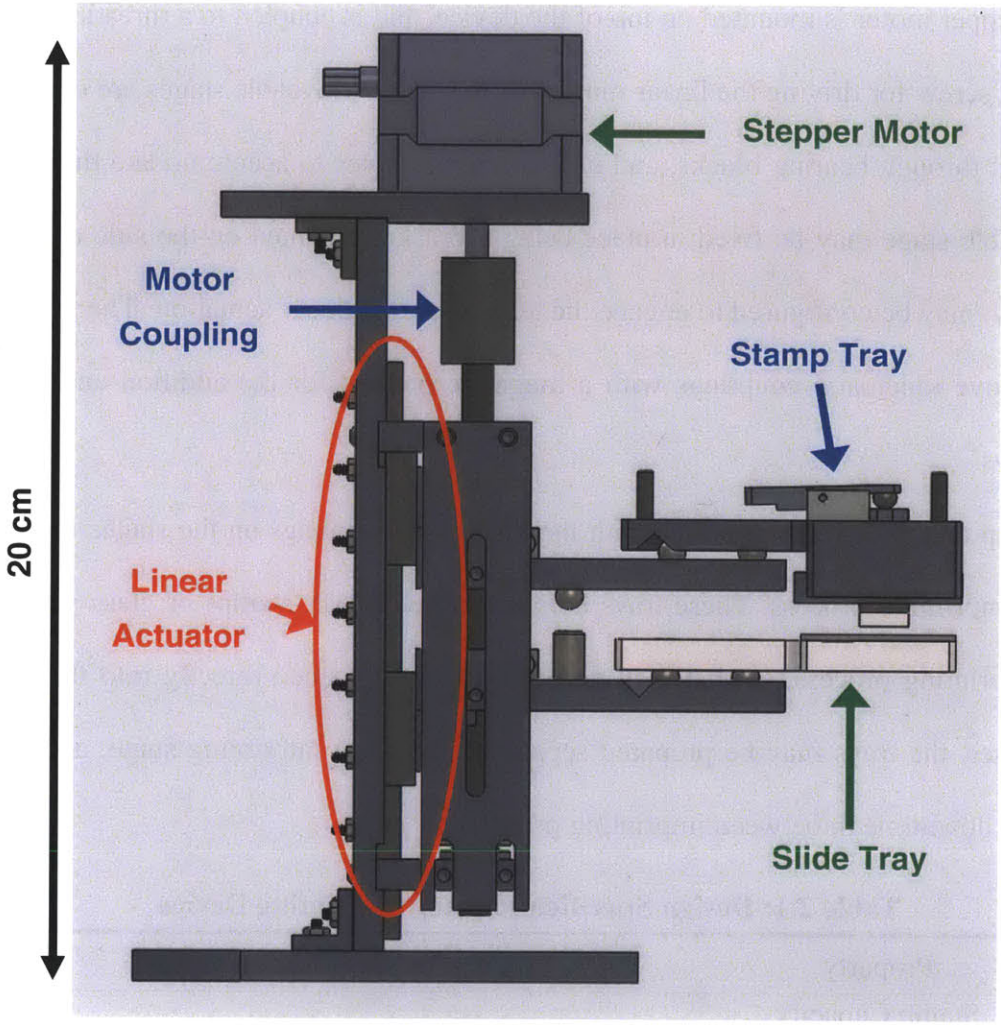

Figure 2.2: CAD diagram of the designed imprinting device with major features labeled.

2.2 Critical Components

The device has three critical areas of design: a linear actuating stage, to provide the translational motion required for the imprinting process; interchangeable trays to hold the stamps and slides; and a set of features designed to facilitate automation of the imprinting apparatus.

2.2.1 Linear Actuating Stage

At the heart of the imprinting device is the linear actuation mechanism. This device uses a vertically-mounted precision ground rail and bearing blocks for linear motion. The precision rail is mounted onto an aluminum plate which serves as the backbone of the device, providing structural support for the entire device. By using the precision rail as the point of attachment for the stages, it is ensured that they travel along the same axis, simplifying the overall alignment effort.

Table 2.2: Linear Actuating Stage Design Goals.

Property	Goal
Precision Rail Length	100 mm
Force Requirements of Actuator	$3 - 5$ N
Stroke Length	> 15 mm
Resolution of Linear Motion	3.25 μm
Speed	< 1 mm/s

The imprinting process requires precise control of the movement of the stage, to reduce the potential for damaging contact forces. As a result, a stepper motor was selected to provide the input for the motion of the moving stage. A lead screw was selected as the driving mechanism for the linear travel, particularly due to the high mechanical advantage afforded by a lead screw. In addition, the self-locking property of a lead screw mechanism is desirable to maintain the position of the stage at a constant height. The motor is mounted at the top of the device with the shaft facing downwards, parallel to the precision rail. The motor is coupled to the lead screw via a flexible coupling, and the lead screw passes through both stages of the device.

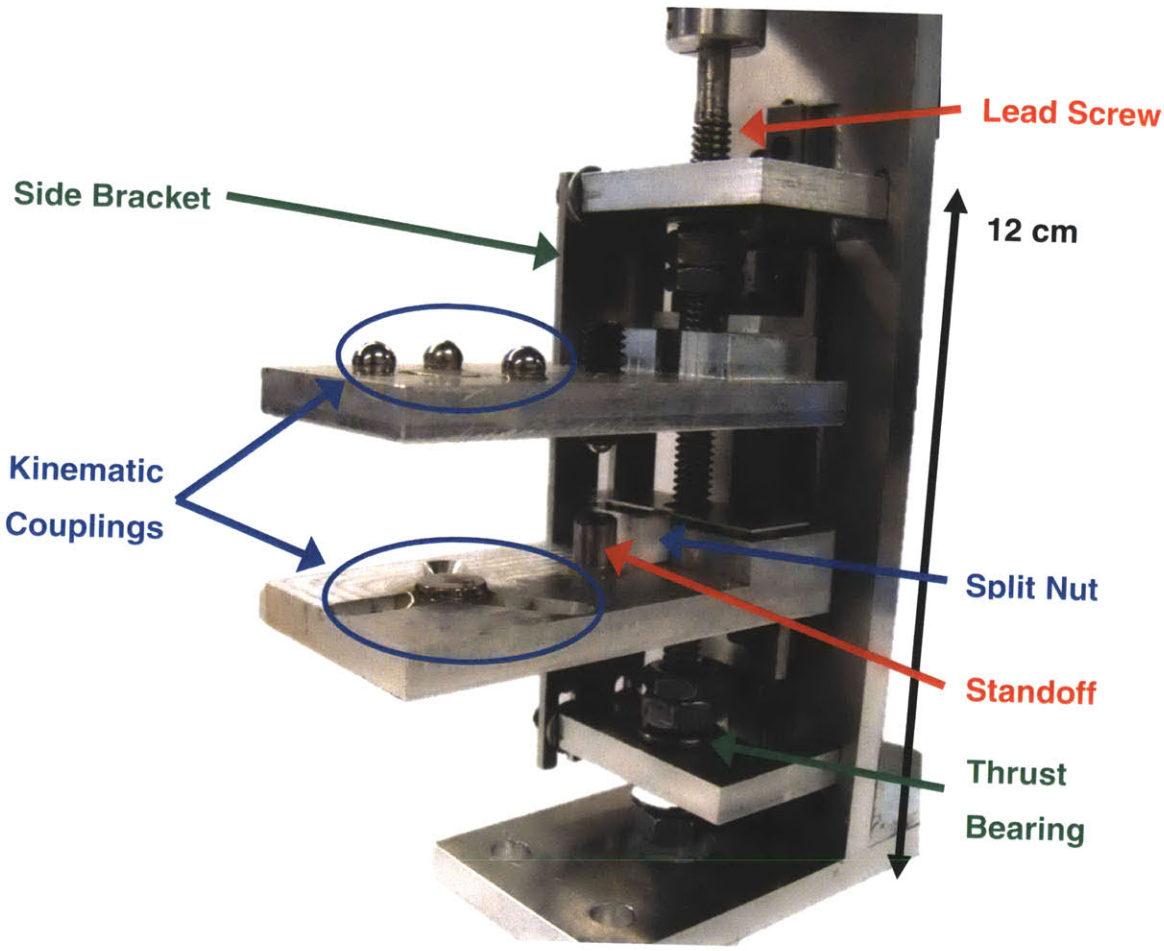

Figure 2.3: Photograph of the fabricated linear actuation mechanism.

To support the lead screw and hold the stationary stage in place, a pair of bearing mounts was added to the device. A pair of thrust bearings is utilized at each end to provide smooth rotation of the lead screw, and locknuts provide the preload necessary to keep the lead screw constrained. To fix the stationary stage in place, an aluminum bracket connects the two bearing holders, and features a slot through which a screw can lock the stage in place.

To engage the lead screw and provide no slip, a square, flexible split nut was introduced into the design. The square nut was fabricated from Teflon for low-friction operation. Because the device must be easily reconfigurable, both the top and bottom stages feature pockets for the

square nut, allowing configuration of the lead screw to drive either the top or the bottom stage depending on the desired method of operation.

The gap between the top and bottom stages when the device is closed is determined by a dowel pin standoff extending above the bottom stage. To permit adjustment of this gap, an adjustable, ball-tipped screw extends underneath the top stage. In conjunction with the dowel pin standoff, this creates physical contact to indicate that the desired position has been reached. It is also desirable that the linear travel of the stage stop when the ball makes contact with the pillar, so the pillar is electrically isolated. Consequently, the ball and pillar interface serves not only as a physical stopping barrier, but also acts as an electrical switch. When the ball contacts the pillar, the circuit is closed, which may be interpreted as a "stop" command to the controller.

The imprinting stage is designed to operate as a base for interchangeable trays to hold stamps and slides, which are described in Section 2.2.2 below. Both the top and bottom stages feature either precision balls or grooves for a 3 ball and 3 v-groove kinematic coupling. This common interface enables rapid reconfiguration of the system to utilize different arrangements or numbers of stamps and slides through the replacement of stamp and slide holder trays.

2.2.2 Interchangeable Stamp and Slide Trays

The flexibility of the imprinting device is primarily accomplished by the use of interchangeable stamp and slide trays. These trays interface with the kinematic couplings on the linear motion stage, allowing for modular replacement of components to change the device function or operating method. If a new slide or stamp layout or quantity is desired, then it is only necessary to fabricate new trays. This interface was also chosen because kinematic couplings are highly repeatable, which is required to produce consistent alignment between stages.

To maintain contact and ensure a firm seating of the kinematic coupling, a magnetic preload was added to each coupling. Magnets were placed at the center of the coupling on both pieces, so that when the coupling was engaged, the small gap between the magnets would ensure strong magnetic force. While mechanical fasteners or other types of preloading would also have been sufficient, the magnetic preload was chosen for its ease of engagement, as they are readily added and removed by an operator, much more easily than could be done with a bolt or screw-based preload.

2.2.2.1 Stamp Tray Design

Because a major goal of the imprinter design was to demonstrate that it can scale up with minimal adjustments, the stamp tray which was designed and fabricated supports 3 PDMS stamps. The stamps sit on aluminum holders, to avoid directly handling the stamps, and the stamp holder assemblies are loaded into the 3 cavities on the tray, as seen in Figure 2.4. A cover is then fastened to the tray to contain the stamps so they may be inverted for the imprinting process.

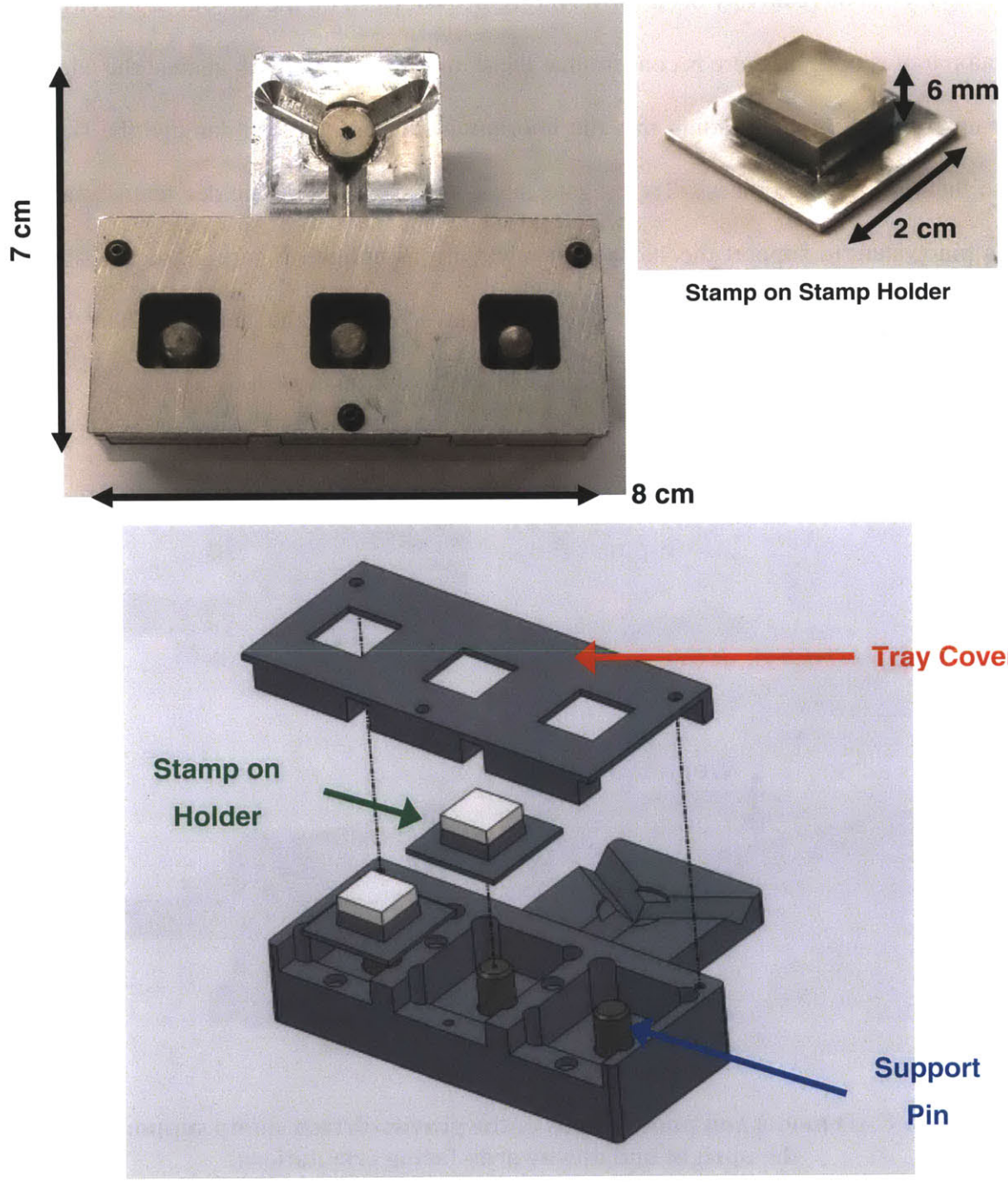

Figure 2.4: Photograph of the fabricated and assembled stamp tray and stamp holder, and exploded CAD model of the main component of the stamp tray

For the self-alignment of the stamps to function properly, it is necessary for the stamp holder cavities to be relatively deep. However, if the stamps sit on the bottom of the cavity when the stamp tray is upright, there is concern that the stamp surfaces will rub against the edges of the cover upon inversion and loading into the imprinting stage, which can damage the stamps and reduce the yield of the process. To mitigate this concern, the stamp holder features a gravity-driven pin system to support the stamps when the tray is upright. Figure 2.5 demonstrates this mechanism, which uses a lever to provide an upwards force on the stamps. When the tray is inverted, the force is removed, and the stamps are free to self-align as designed.

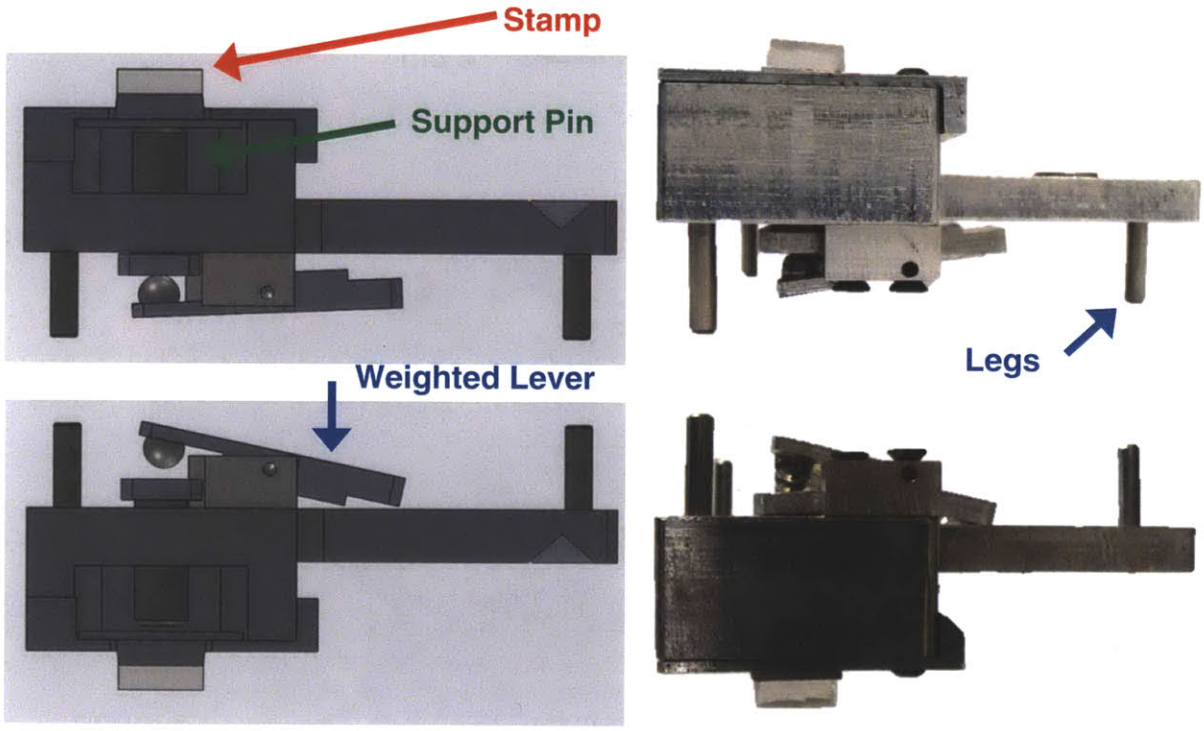

Figure 2.5: CAD model and photographs of the gravity-driven stamp support system in the upright and downwards-facing orientations.

In order to provide a stable platform when loading and unloading stamps from the tray, a set of 3 pins was added to the back of the tray. These pins allow the stamp holder to be placed on a table for loading without wobbling, and protect the pin mechanism.

Table 2.3 lists design specifications for the stamp tray. The tray is designed to hold 3 stamps on stamp holders (shown in Figure 2.4) not only during the imprinting process, but also during the preceding gold deposition process (discussed further in Section 2.2.3). Consequently, the stamp tray is limited both in its maximum outer dimensions (to fit into the gold sputterer) and the outer dimension of the stamp area (to ensure the stamps fit beneath the gold deposition region of the sputterer).

Table 2.3: Stamp Tray Design Goals

Property	Goal
Stamp Capacity	3
Stamp Holder Dimensions	20 mm × 20 mm
Stamp Dimensions	10 mm × 10 mm × 3.25 ± 0.07 mm
Maximum Diameter of circle circumscribing the Stamps Arrangement	60 mm
Maximum Outer Diameter of Tray	144 mm

2.2.2.2 Slide Tray Design

The tray for holding the glass slides, shown in Figure 2.6, has fewer features than the stamp tray. Like the stamp tray, it features a removable lid to restrain the glass slides from being pulled from the tray after the imprinting process is complete. To facilitate the transmission of UV light from beneath the imprinter, the slide tray was designed with large holes beneath each slide position. To constrain the slides in plane, the tray has shallow pockets machined into its surface, providing alignment edges for the slides. Table 2.4 highlights the major design specifications for the slide tray.

Table 2.4: Slide Tray Design Goals

Property	Goal
Slide Capacity	3
Glass Slide Dimensions	22 mm × 22 mm × 0.15 ± 0.02 mm
Hole Size for UV Light	21 mm × 21 mm

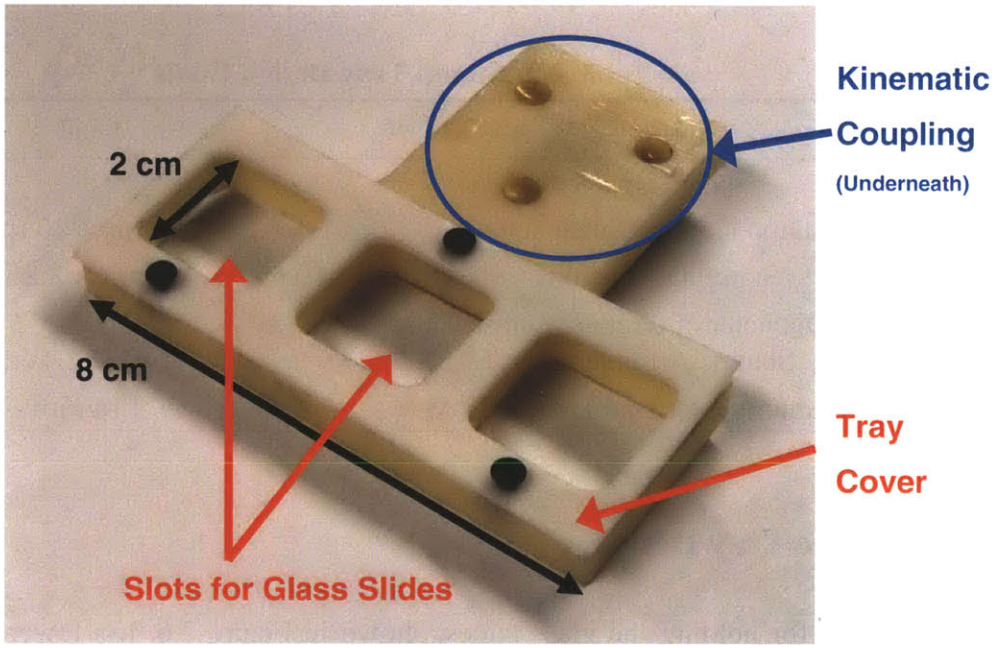

Figure 2.6: Photograph of the fabricated and assembled slide tray.

2.2.3 Automation

While not a physical component of the system, much of the system design is motivated by the need for automation. Ultimately, the imprinting apparatus will be incorporated into an entire automated process, which presents several unique challenges that the design of the imprinter must address.

To permit the transition from the gold deposition process to the imprinting process, the imprinter was designed to use modular stamp and slide trays, as discussed in Section 2.2.2. The

stamp tray in particular was heavily influenced by the need for automation. The support pins and stand built into the tray were chosen to allow for ease of loading and unloading of the tray. Further, due to the fragility of the stamps from the combing process onwards, the tray is designed to accommodate the stamps for the entire process. The pins ensure that the stamps are exposed for both the combing and gold deposition process, and the entire tray is sized to fit within the gold sputterer to be used in tests.

In consideration of the eventual need for an automated polymer dispensing solution, the stamps and slide trays are arranged linearly, so that a dispensing module with linear travel may be utilized to automate the process. A circular stamp layout was also considered, but the decision to use a linear slide and stamp arrangement was made so that the device would scale better. Increasing the scale of a linear system only requires that the dispensing system be extended in 1 direction of travel, while a circular arrangement would require at least 2 degrees of movement.

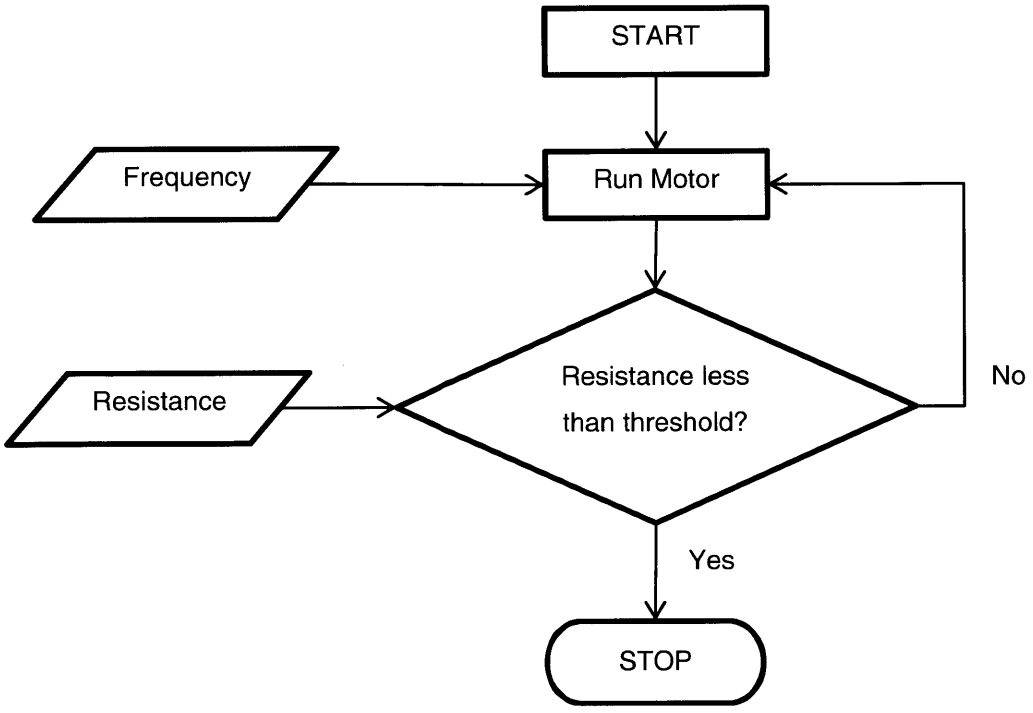

Figure 2.7: Process flow of method used to control actuation of the stage.

Finally, for both ease of use and to demonstrate the ability to be controlled as part of an automated process, the imprinting motion of the fabricated device was controlled using LabView.[5] By using a LabView VI to drive the stepper motor and implement the contact switch, the device may be easily programmed to run not only as a standalone unit, but also as part of an entirely automated process, controlled by a central program, such as LabView. Figure 2.7 shows a block diagram of a basic program used to control the motion of the device.

The contact switch is implemented as a resistance threshold, where the LabView program monitors the resistance across the ball and pillar. Because the pillar is isolated from the rest of the system, no current flows when the stages are apart, and the resistance is infinite. When the ball makes contact with the pillar, the circuit is closed, current flows, and LabView can measure the resistance across the circuit. When the measured resistance drops below a user-defined threshold indicating contact has been made, the motor is stopped.

The stepper motor responds to a square wave input, making 1 step for each rising edge. Each step consists of a rotation of a fixed step angle ϕ, which depends on the configuration of the motor controller and the specifications of the motor itself. The velocity of the linear actuation is adjusted by changing the frequency f of the step function, increasing the number of steps per second. Finally, the length traveled per angle of rotation, or the linear displacement resolution of the stage, ℓ, can be determined Using this information, the linear actuation velocity of a stepper motor driven lead screw may be evaluated as:

$$v_{linear} = f\phi\ell \tag{2.1}$$

The pitch of the lead screw is known, and is defined as the number of threads per unit length. This allows the calculation of ℓ:

$$\ell = \frac{\text{length}}{\#\ \text{threads}} \times \frac{1\ \text{thread}}{360°} \tag{2.2}$$

The displacement resolution of the actuator is determined by the linear resolution and the step angle:

$$r_{displacement} = \phi\ell \tag{2.3}$$

This device utilizes a ¼-20 lead screw, for which $\ell = 3.53\ \mu m/deg$. The Vexta PK243-01AA stepper motor used in this device has a basic step angle of 1.8°, and the Interinar BSD-013G-8 motor controller used for this device is configured to eighth-step mode.[3],[4] Consequently, for this device, $\phi = 0.225°$; using Equation (2.3), the $r_{displacement}$ for this device is found to be $0.794\ \mu m$.

Thus, the linear velocity of this imprinting stage is defined by the function:

$$v_{linear} = 0.794f\ {}^{\mu m}/_{s} \tag{2.4}$$

The stepper motor on this device is expected to be driven at about $200 - 400$ Hz. As a result, anticipated imprinting velocities range from approximately $160 - 320\ {}^{\mu m}/_{s}$. Assuming a total imprinting stroke of 1 cm and a UV curing time of 15 minutes, the expected cycle time for a full imprinting process (excluding dispensing time) is $16 - 17$ minutes.

2.3 Scalability Metrics and Model

Because the focus of this work is the relationship between performance and scale of the process, it is important to identify which components have the greatest impact on scale and performance of the device, and how to measure their effects on the device scale and performance. The maximum scalability of this device lies at the point where it can produce the maximum number of parts that meet minimum quality requirements, all while staying within the

desired operating constraints. This work focuses on the performance of two aspects of the device in the determination of its scalability: (i) the kinematic couplings and fixtures, and (ii) the linear motion stage.

2.3.1 Kinematic Couplings and Fixtures

The stages' kinematic couplings are vital to quality performance of the device, as they serve as the interface between the trays and the linear actuator. The most important characteristic of a kinematic coupling is its repeatability. Because the ball-and-groove kinematic couplings used in this device are designed to constrain 6 degrees of freedom, they should settle in the same position every time, with very little variation. This is crucial for yielding products of consistent quality, which is why it is one of the metrics used to evaluate this device.

Inconsistent alignment and high variations in the seating of the kinematic coupling can greatly reduce the performance of the system. In-plane rotation and translation can prevent stamps or slides from engaging properly, resulting in damaged stamps or defective final products. Additionally, any roll or pitch variations in the seating of the kinematic couplings can reduce the yield of the system. A tray with a high enough roll variation can cause a stamp at one end to make contact with the slide, while a stamp at the other end does not. Figure 2.8 demonstrates this effect when the trays are offset from parallel by an angle θ.

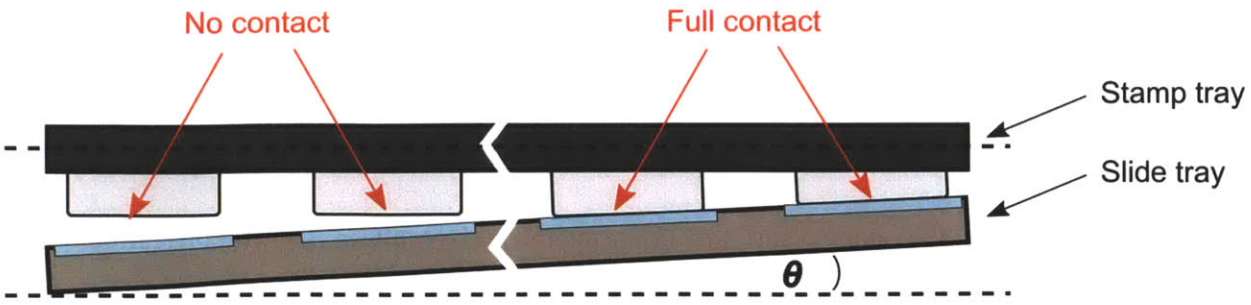

Figure 2.8: The effect of nonparallelism on the scale of production. The slide tray is offset from horizontal by an angle θ.

Initial nonparallelism of the stages, stamps, and slides is another major factor determining the scalability of an imprinting device. There are 3 major sources of initial misalignment errors: (i) misalignments between the trays/stages; (ii) misalignments between the stamp holders and their tray; and (iii) misalignments between the slides and their tray. The stage misalignment is primarily a function of the quality of the kinematic coupling and the fixed alignment of the device, while the other two misalignments are determined by the quality of the fixtures holding the stamps and slides in their respective trays. In addition, the quality of machining affects all 3 of these misalignments, as the repeatability and precision of the machine or fabrication method introduce errors and misalignments between parts of the system.

2.3.2 Stage Motion

The other property to be observed as an evaluation of scalability is the motion of the linear actuator and the stage in motion. As was discussed in Section 1.1.2, in-plane movement of the stamps should be minimized, as the gold-plated DNA nanostrands are highly prone to damage. While improperly designed kinematic couplings can provide static in-plane variations in rotation and translation, dynamic in-plane motion of the linear stage is much more likely to cause damage to the stamps.

Further, because the kinematic couplings are attached to the stages, any nonparallelism between the two stages runs the risk of being amplified due to variations in the kinematic couplings, causing the stamp and slide trays to act as moment arms. Small variations in the performance of both the stages and the couplings could result in significant reductions in performance and quality of the process, and it is important to understand the limitations of the device.

2.3.3 Scalability Model

The aforementioned metrics may be combined into a single model for ease of analysis, allowing quick evaluation of a device's scalability based on the definition of scalability used here.

The stages have two main states: open and closed. In the open state, shown in Figure 2.9, a stamp tray of length l is used over a slide tray offset by angle θ_{stage}. h_{open} is defined to be the measured minimum distance between the two trays, and h_0 to be the arbitrary minimum gap between the trays. This gap serves as a safety buffer between the trays during the loading process, to mitigate the chance of damage to stamps during loading into the imprinting device. In addition, t is defined as the thickness of the stamp/holder assembly relative to the lid of the stamp tray.

Angular misalignments between the stamps, slides, and their respective trays are denoted as θ_{stamp} and θ_{slide}, respectively. Similarly, δ_{stamp} and δ_{slide} describe the thickness variations of the stamp and slide. Assuming the worst case of misalignments, the stamps and slides are misaligned in the manner shown in Figure 2.9. In addition, the assumption of worst case analysis extends to the stamp and slide thicknesses, and it is assumed that the thinnest stamp and slide are located as far apart as possible, with the thickest of each located closest together.

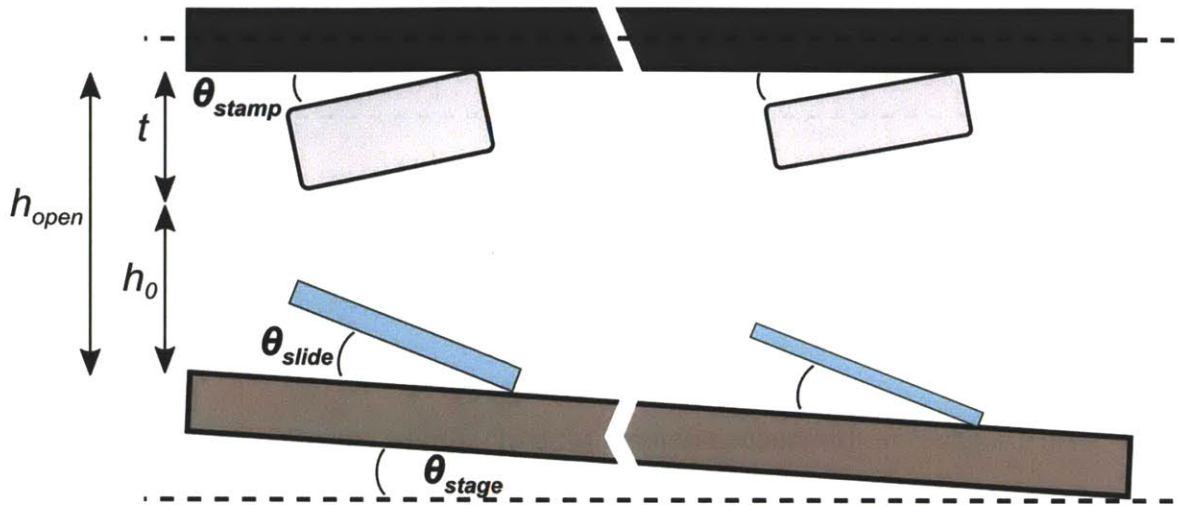

Figure 2.9: Diagram of trays in the open state, with key dimensions defined.

The difference in height between the thickest and thinnest stamps and slides is denoted by d_{stamp} and d_{slide}. For the stamps, this difference is determined using the relationship shown in Figure 2.10; the stamps are assumed to be both vertically offset by twice their variation in thickness δ_{stamp}, and misaligned by angle θ_{stamp}. Consequently:

$$d_{stamp} = 2\left(l_{stamp} \sin \theta_{stamp} + \delta_{stamp}\right) \tag{2.5}$$

Relative to the slide tray, d_{slide} is determined using a similar relationship. However, since the misalignment θ_{stage} is defined as acting on the slide holder, it is necessary to account for the misalignment of the slide stage when determining d_{slide}:

$$d_{slide} = 2 \cos \theta_{stage} \left(l_{stamp} \sin \theta_{stamp} + \delta_{stamp}\right) + l \sin \theta_{stage} \tag{2.6}$$

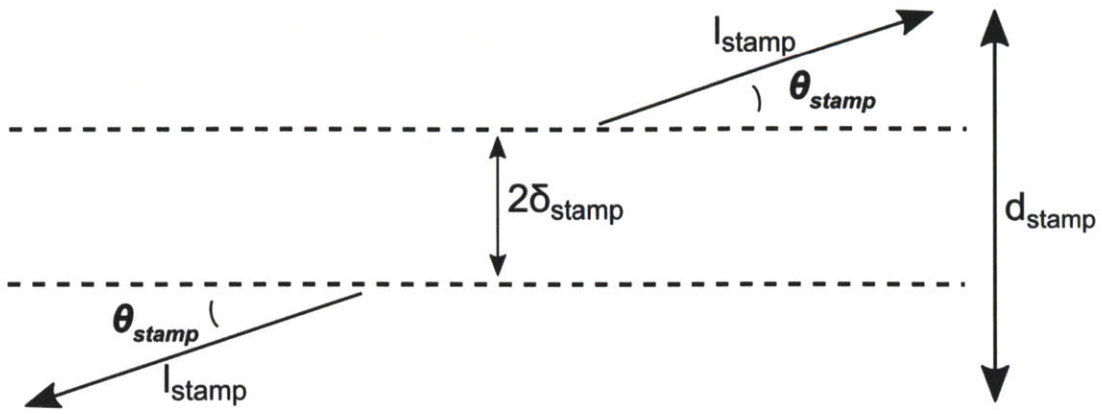

Figure 2.10: Diagram of dimensions determining maximum variation in stamp height.

In the closed state, shown in Figure 2.11, h_{closed} is defined as the distance between the closed trays, which allows the model to account for access for a dispensing nozzle for the polymer. In addition, the value h_{min} is chosen to be the minimum value for h_{closed}; this parameter is used to specify the minimum gap between the stages, to ensure access for a dispensing nozzle or similar instrument. Another parameter, l, is defined as the length between the centers of the end slides.

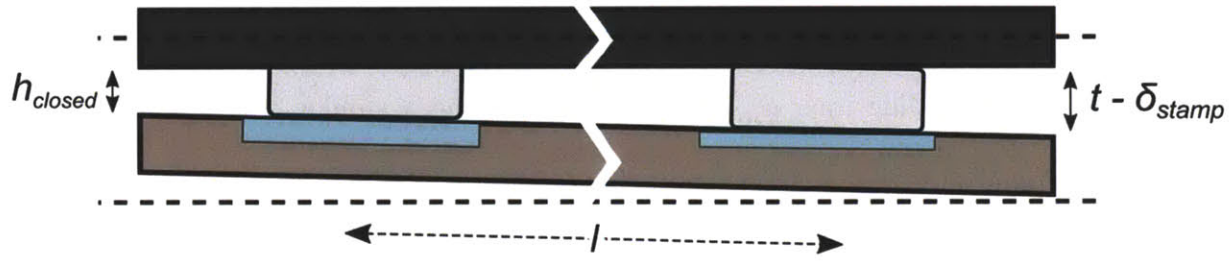

Figure 2.11: Diagram of trays in the closed state, with key dimensions defined.

Based on the linear design of the trays, a value k for the system is chosen to represent the tray length required for a single stamp/slide pair. Using this value, the scale of the system can be obtained in terms of the quantity N of chips that can be produced under the given parameters:

$$N = \frac{l}{k} + 1 \tag{2.7}$$

The misalignment effects on the system, y, are modeled by combining Equations (2.5) and (2.6):

$$\begin{aligned} y = {} & 2\cos\theta_{stage}\left(l_{slide}\sin\theta_{slide} + \delta_{slide}\right) + l\sin\theta_{stage} \\ & + 2\left(l_{stamp}\sin\theta_{stamp} + \delta_{stamp}\right) \end{aligned} \tag{2.8}$$

To model the scalability of the device, the maximum possible height drop of the slide tray over its length due to misalignments (which still results in successful imprinting) must be determined. In this scenario, one end of the lower tray is h_{min} from the upper tray, and the other end of the tray is the maximum distance it can be from the upper tray while still making contact with the thinnest stamp. Consequently, the end of the tray is modeled to be $t - \delta_{stamp}$ from the other tray.

This places a condition on the system:

$$y \leq t - \delta_{stamp} - h_{min} \tag{2.9}$$

Thus, the scalability of a system may be determined by evaluating the misalignment effects using Equation (2.8), and ensuring that the condition of Equation (2.9) is met.

Combining and rearranging Equations (2.8) and (2.9) provides a parameter for l:

$$\begin{aligned} l \leq {} & \frac{t - \delta_{stamp} - h_{min} - 2\cos\theta_{stage}\left(l_{slide}\sin\theta_{slide} + \delta_{slide}\right)}{\sin\theta_{stage}} \\ & - \frac{2\left(l_{stamp}\sin\theta_{stamp} + \delta_{stamp}\right)}{\sin\theta_{stage}} \end{aligned} \tag{2.10}$$

Substituting into Equation (2.7), the number of chips N that can be produced is expressed by:

$$N \leq \frac{1}{k \sin \theta_{stage}} \left[t - \delta_{stamp} - h_{min} \right.$$
$$- 2 \cos \theta_{stage} \left(l_{slide} \sin \theta_{slide} + \delta_{slide} \right) \tag{2.11}$$
$$\left. - 2\left(l_{stamp} \sin \theta_{stamp} + \delta_{stamp} \right) \right] + 1$$

Finally, the length z_{act} of actuation that the stage must travel for a complete imprinting cycle is evaluated:

$$z_{act} = h_{open} - h_{closed} \tag{2.12}$$

While this is not directly tied to the scalability of the system, this parameter does help to determine the scale by determining whether the amount of linear travel necessary for the imprinting cycle is achievable given the design of the device.

CHAPTER

3

EXPERIMENTS AND ANALYSIS

3.1 Kinematic Coupling Repeatability

3.1.1 Measurements and Analysis

Examination of the kinematic couplings used in the stage-tray interface found that the kinematic couplings were repeatable to within tens of micrometers and microradians, or less. Table 3.1 has the results of the metrics measured to determine the repeatability of the couplings, as well as the measurement resolutions. As the results show, the repeatability of all aspects of the kinematic couplings exceeded the resolution of the dial gages used in measurement (12.7 μm.).

Table 3.1: Repeatability of Kinematic Couplings

Direction	Stamp Holder	Slide Holder
X Translation	-0.90 ± 12.7 μm.	0.48 ± 12.7 μm.
Y Translation	3.1 ± 12.7 μm.	4.2 ± 12.7 μm.
Z Translation	2.85 ± 12.7 μm.	5.13 ± 12.7 μm.
In-Plane Rotation	16.7 ± 35.1 μrad.	10.2 ± 48.4 μrad.
Roll	37.2 ± 333 μrad.	67.2 ± 333 μrad.
Pitch	72.8 ± 364 μrad.	46.1 ± 364 μrad.

Because the repeatability exceeds the resolution of the gages, the conclusions that may be drawn are limited. However, it may be concluded that they are at least as repeatable as the resolution of the gages, which gives a reference point to work from. Based on this assumption,

the repeatability of the kinematic couplings is not a major factor contributing to misalignments of the device, because in order to achieve significant misalignments due to variations on the order of the measurement resolution, the stage would need to be prohibitively large in size. Using trigonometric relationships to analyze the effects of variations, in order to undergo a 1 mm translation due to rotational or translational variations, the tray would need to exceed 1 m in dimension.

3.1.2 Experimental Procedure

In order to accurately determine the repeatability of the kinematic coupling, three sets of measurements were taken for each tray. First, a group of 3 dial gauges were used around the edges of the trays to observe their rotation and translation in the xy-plane. Secondly, a pair of dial gauges was used on the bottom surface of the tray to evaluate the roll and pitch of the tray about its axes of symmetry. These measurements also were used to determine the out-of-plane z-translation of the tray.

For each set of measurements, a tray from the imprinting stage, separated from the main device, is fixed to a measurement stage, which is in turn attached to the lab table. This locks the orientation of the stage relative to the table, and consequently, attaching the gauges to the table places them in the same reference frame. Figure 3.1 is an example of an experimental setup used.

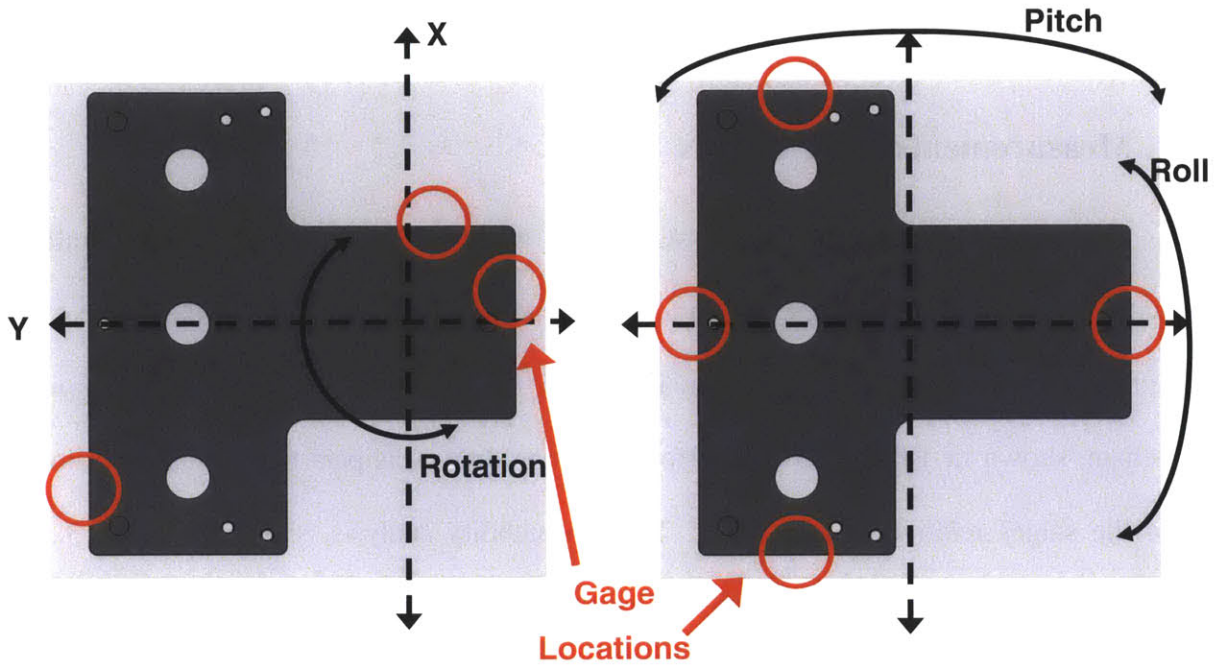

Figure 3.1: Measurement points and rotational axes used in the kinematic coupling repeatability experiments.

3.2 Estimation of Fixture Misalignments

While precision fixturing of the stamps and slides was not a focus of this thesis, it is worth a quick analysis because as discussed in 2.3.1, these factors determine the parameters θ_{stamp} and θ_{slide} in the scalability model.

Fabrication for this device was performed on an Intelitek Benchman MX, which performs with an accuracy of $\delta_{fab} = 5$ μm.[6] Fixture misalignments would be most relevant over the opening in the stamp tray lid and the UV light hole in the slide tray, as these are surfaces on which the stamp holder and slides rest. Assuming a maximum variation in fabrication of 2δ, θ_{stamp} and θ_{slide} are estimated to be 1000 mrad and 470 mrad, respectively.

3.3 Characterization of Stage Motion

3.3.1 Measurements and Analysis

The motion of the imprinting stage was analyzed in terms of initial parallelism, repeatability over multiple cycles, and in terms of parasitic motions within cycles. One cycle is defined as the movement from an open imprinter, to closed, then back to open again. The parallelism, shown in Table 3.2, was performed using digital calipers to measure the pitch and roll of the stages relative to each other. The repeatability analysis, shown in Table 3.3, was performed using similar methods as those employed in the kinematic coupling analysis, and represents variations in the stage position from cycle to cycle. However, because the stage was measured in motion, it was not possible to measure the roll and pitch variations of the stage using the same methods, and these variations are unknown. The parasitic motion analysis, shown in Table 3.4, represents variation in the tray's translation and rotation when traveling from the open position to the closed position.

Table 3.2: Parallelism of Linear Stages

Direction	Angle
Roll	650 ± 390 μrad.
Pitch	2.46 ± 0.47 mrad.

Table 3.3: Repeatability of Linear Stage Motion Over Multiple Cycles

Direction	Open	Closed
X Translation	0.60 ± 12.7 μm.	0.55 ± 12.7 μm.
Y Translation	-0.07 ± 12.7 μm.	-0.06 ± 12.7 μm.
In-Plane Rotation	11.2 ± 70.9 μrad.	10.1 ± 32.5 μrad.

Table 3.4: Parasitic Motion of Linear Stage During Imprinting Cycles

Direction	Average Variations
X Translation	0.06 ± 12.7 μm.
Y Translation	-0.006 ± 12.7 μm.
In-Plane Rotation	-1.02 ± 70.9 μrad.

The parallelism of the stages was found to not be of significant concern. After a first round of measurements showed that the trays severely rolled from side to side, the trays were adjusted and remeasured, demonstrating an average drop of 0.02 mm from side to side, and an average drop of 0.14 mm from front to back.

Once again, it appears that the repeatability performance is better than the resolution of the dial gages used. From cycle to cycle, the lower stage holding the slide tray experiences small transient rotations. These are very slight movements, and should not significantly affect the scalability of the device. Similarly, the variations in x- and y- positions, measured as translations, were very low for the linear stage. While the resolution of the data is limited, this still allows the conclusion that the repeatability of the stage's position from cycle to cycle is very high, and should have little effect on the scalability of the device.

In the parasitic motion analysis, it was found that the x- and y- translations during the transition from open to closed were very low, and once again, may have been outside of the resolution of the measurements. Similarly, it was found that on average, the in-plane parasitic rotation is smaller than the measurement resolution, and likely has a negligible effect on the scalability of the device.

3.3.2 Experimental Procedure

First, the parallelism of the two stages was determined using measurements with digital calipers The stepper motor was cycled through a simulated imprinting operation, stopping at both

the top and bottom of its travel ("open" and "closed"), and measurements were made to identify the distance between corresponding points on the upper and lower stages. Much as with the pitch and roll of the kinematic couplings, these measurements were used to determine the relative tilts between the upper and lower stages about the x- and y-axes. However, differently from the kinematic coupling analysis, these measurements were not used for extensive analysis, but were used to adjust the stages to be as parallel as possible before proceeding to measure the in-plane movements of the stages.

Secondly, the in-plane movement of the moving stage was measured using methods similar to those used in evaluating the kinematic couplings. Dial indicators were placed along the edges of the moving stage as shown in Figure 3.2, and measurements were taken in both the open and closed positions. Using the same algorithm as described in Section 3.1.2, the rotational and translational variations were calculated, to provide insight on the in-plane movements of the stage as it moved through a simulated imprinting process.

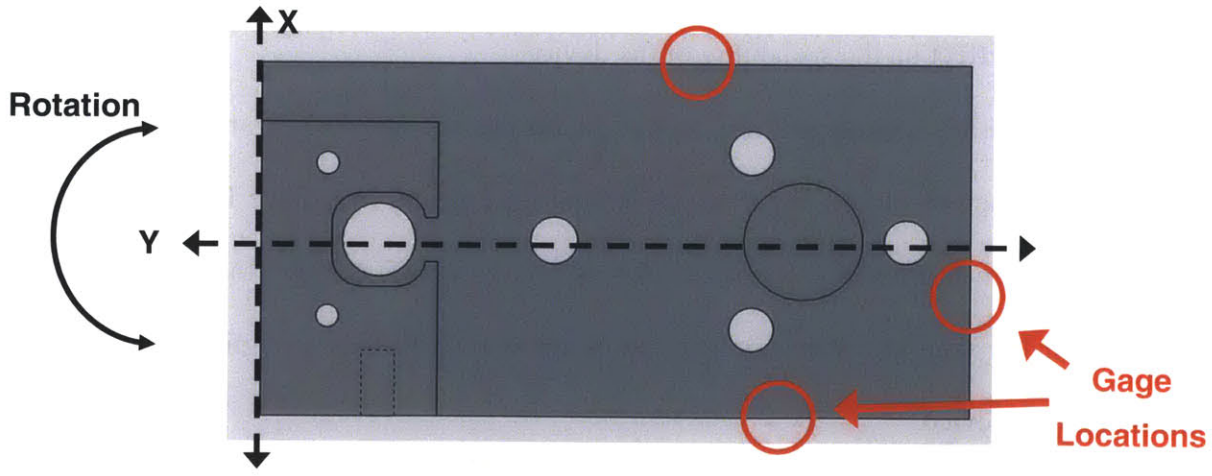

Figure 3.2: Diagram of experimental setup for characterization of linear motion

3.4 Magnetic Preload Force

3.4.1 Measurements and Analysis

To better understand the performance of the imprinting device, the strength of the magnetic preloads used to hold the kinematic couplings together were measured, along with the mass of each tray. The results are shown in Table 3.5.

Table 3.5: Magnetic Preload Force of Kinematic Couplings

Measurement	Stamp Tray	Slide Tray
Preload Force	5.01 ± 0.28 N	4.25 ± 0.16 N
Mass	131 ± 1 g	22 ± 1 g

3.4.2 Experimental Procedure

Force measurements were taken using an electronic force sensor. As shown in Figure 3.3, the stage was secured to the lab bench using the fixture designed for measurement of the kinematic coupling repeatability. The force sensor was attached to the corresponding tray, centered over the kinematic coupling. The sensor was then lifted vertically out until the coupling separated, and the force required was recorded.

Both couplings were found to be about the same strength; however, the mass of the stamp tray is much larger than that of the slide tray. As a result, the stamp tray coupling is significantly weaker than the slide tray coupling, as the heavier stamp tray exerts a much greater moment on its coupling. Consequently, although the stamp tray coupling joins and holds in a repeatable manner, it is easily jostled loose. Because of the fragility of the nanostrands on the stamps, it is recommended that stronger magnets be used in the stamp tray kinematic coupling.

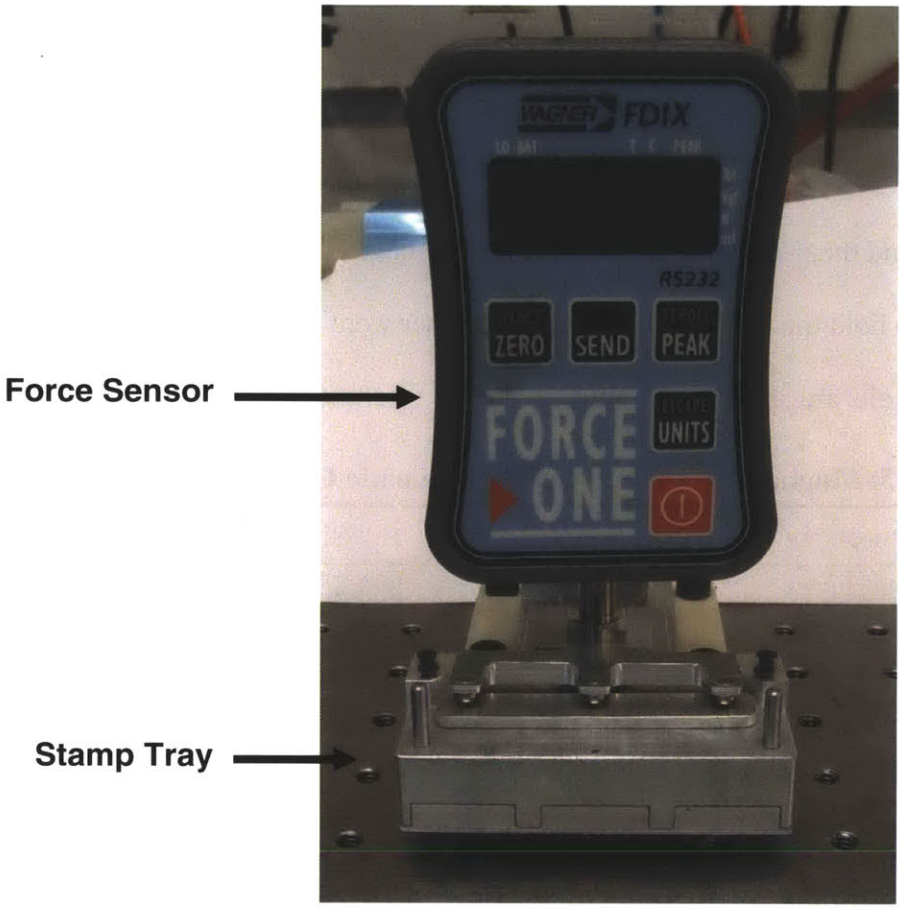

Figure 3.3: Experimental setup for measurement of magnetic preload force

CHAPTER

4

IMPRINTING AND SCALE ANALYSIS

4.1 Scalability Analysis

The scalability of the device can be determined using the scalability model developed in Section 2.3.3. This can be accomplished by determining the maximum acceptable misalignments for θ_{stages}, θ_{stamp}, and θ_{slide}. This device was designed to accommodate $N = 3$ stamps, and with the device accommodating 1 stamp/slide pair every 26 mm, $l = 52$ mm. For this analysis, $h_{min} = 4.5$ mm.

Other parameters were derived from the design specifications of the device: $t = 8$ mm; $\delta_{stamp} = 0.07$ mm; $\delta_{slide} = 0.02$ mm; $l_{stamp} = 10$ mm; and $l_{slide} = 19$ mm. These parameters were used with Equations (2.8) and (2.9) to solve for the maximum possible misalignment for each of the three misalignment angles, shown in Table 4.1. Each maximum misalignment was found by setting the other two misalignment angles to 0.

Table 4.1: Maximum Misalignment Angles

Angle	Maximum
θ_{stamp}	0.163 rad (9.3°)
θ_{slide}	0.0856 rad (4.9°)
θ_{stage}	0.0625 rad (3.6°)

This demonstrates that this 3-stamp device has the ability to handle small misalignments in fixturing and stage orientation, and that it should successfully self-align all 3 of the stamps with the slides. The stamp holder is the most forgiving of the alignments, allowing nearly 10° of misalignment before scalability is lost. The stage is the least forgiving, but it is important to note that the stage misalignment is largely determined by the kinematic couplings and linear actuator of the device, which were demonstrated to be highly repeatable in Chapter 3.

4.2 Imprinting Tests

While the model has shown the device to be scalable, a simulated imprinting cycle was performed on the device to better evaluate its performance. Using uncoated stamps and glass slides, the imprinting device was loaded just as it would be for a full imprinting cycle, and the device was run. Qualitatively, the device performed as expected. All three stamps made contact with their respective slides, leaving a gap of approximately 6mm, which would allow access for a dispensing nozzle. This can be seen in Figure 4.1.

The next imprinting test was the inclusion of an intentional misalignment in one of the slides. As shown in Figure 4.2, one side of a slide was propped up, causing a roll misalignment between the slide and stamp. The angular misalignment was approximately $\theta_{slide} = 5°$, which is the upper limit of acceptable misalignments. The imprinting cycle was run again, and in the closed position, it can clearly be seen that all three stamps are once again in contact with the slides, demonstrating the independent self-alignment method used by the stamp holder. The distance between the closed stamp and slide trays was measured to be 4.8 mm, which closely corresponds to the $h_{min} = 4.5$ mm used in Section 4.1 for the scalability analysis; this reinforces the validity of the model.

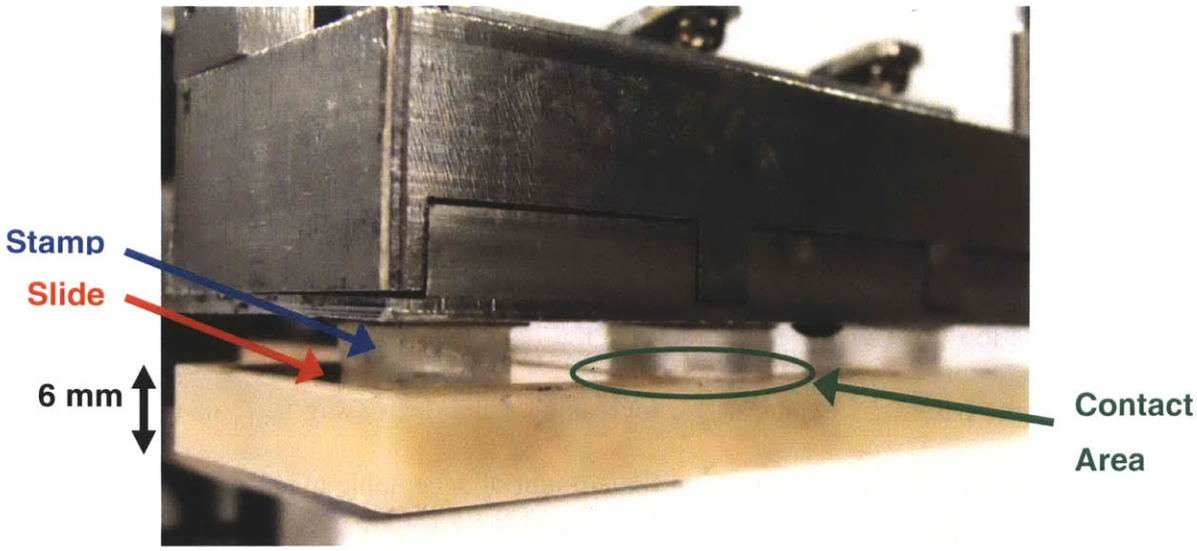

Figure 4.1: Simulated imprinting cycle, demonstrating successful contact between stamps and slides.

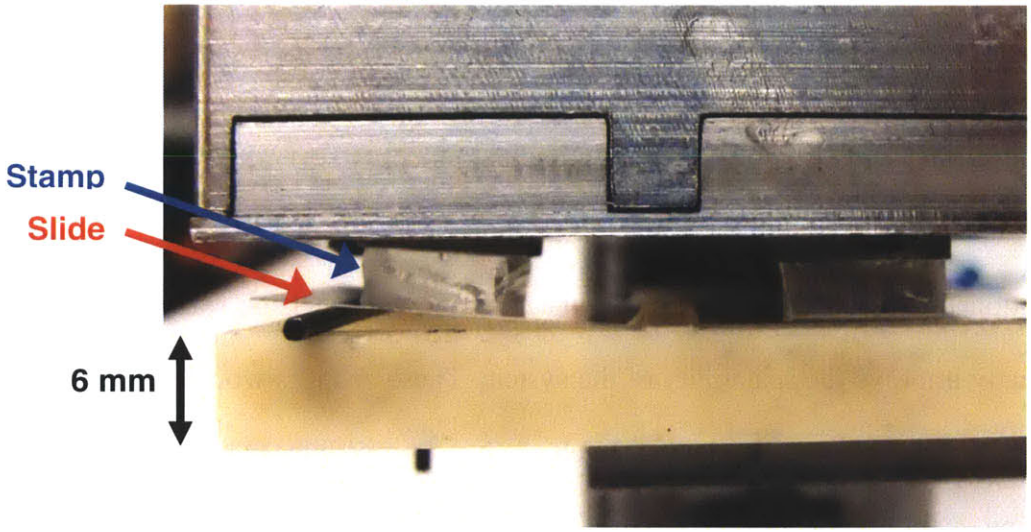

Figure 4.2: Simulated imprinting cycle with intentional misalignment on the leftmost slide, demonstrating the tray's independent self-aligning capability

4.3 Scalability Limitations

Analysis of the imprinting device and the results of the scalability analysis provide some insight into the factors which determine the scalability of the device. The size of the component is a major factor in determining the effect it has on misalignments; the long stamp tray drops the

same amount with a small angular misalignment as the small stamp holder does with a large misalignment. As the size of the stage increases, the system will become less tolerant of small θ_{stage} misalignments, which can be mitigated by improving the quality of the kinematic couplings and the linear motion of the device.

As Equation (2.9) of the model shows, the limits on the scale of the system are largely determined by the parameters t and h_{min}. Increasing t and decreasing h_{min} can greatly increase the scalability of the system by increasing the amount of acceptable misalignment effects. Using the same model as before, increasing the value of t by as little as 2 mm nearly doubles the maximum θ_{stage} for the system, and adds about 5° to the maximum θ_{stamp}.

4.4 Recommended Design Changes

Through the analysis of the results, it is possible to identify several design factors that, if improved, would be likely to improve the scalability of the device.

As mentioned in Section 4.3, increasing the thickness of either the stamps or the stamp holders can greatly improve the scalability of the system. These changes would allow the device to take better advantage of the self-aligning mechanism to permit greater misalignment effects while maintaining quality production.

Another improvement would be better surface finishes inside the kinematic coupling grooves. The aluminum grooves were cut using a chamfer mill, and resulted in grooves with a somewhat uneven finish. Better surface finishes in the grooves decrease the contact area between the ball and groove, making the kinematic coupling more repeatable.

Similarly, the use of stronger materials in the trays would be beneficial. Because the kinematic coupling uses hardened steel balls, there is potential for damage to the corresponding

grooves, which would reduce the repeatability of the coupling. Steel on ABS contact is likely to damage the relatively soft ABS somewhat rapidly, and even the steel-aluminum interface used in this device shows signs of wear. As shown in Figure 4.3, the contact points for the steel balls are visible in the aluminum grooves after repeated separation and connection of the coupling.

Another proposed improvement is the direct mounting of the stages into the linear slide blocks. Currently, the connection is implemented through an angled bracket, but variations in the angle of the bracket and the use of screws, nuts, and bolts as fasteners introduce the potential for nonparallel alignment of the stages relative to each other. Directly mounting the stages onto the bearings reduces the complexity of the connection and reduces the number of factors that can affect the parallelism of the stages.

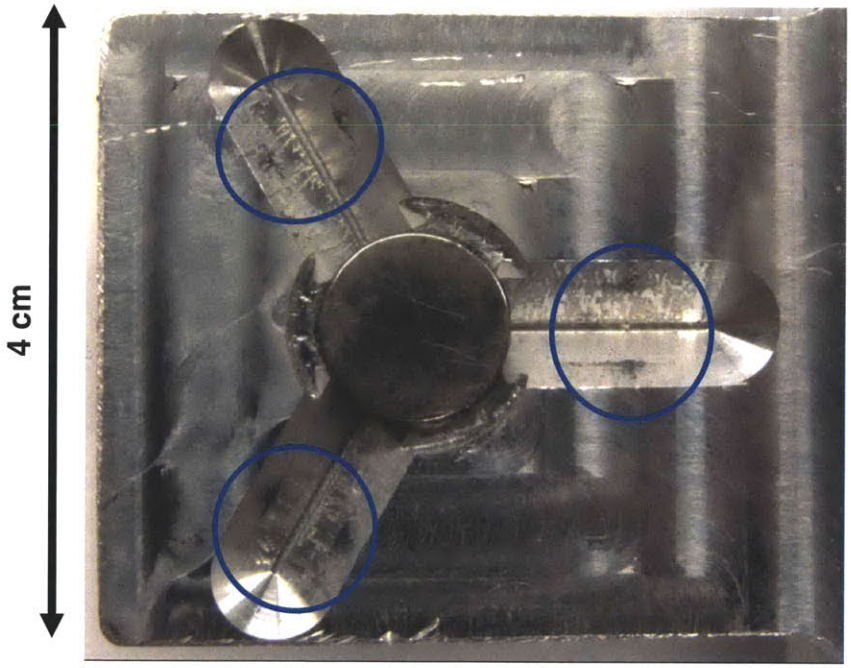

Figure 4.3: Photograph of wear in kinematic coupling grooves

CHAPTER 5

CONCLUSION

5.1 Contributions

Overall, this project met the design goals it set out to satisfy. Table 5.1 provides a comparison of the design specifications to the actual performance of the device.

Table 5.1: Device Design Specifications.

Property	Design goal	Actual device
Automation	Can be incorporated into larger process	Yes
Stamp Capacity	> 1	3
Vertical Travel	$5 - 15$ mm	15 mm+
Height	~150 mm	190 mm
Motion Degrees of Freedom	1	1
Footprint	< 30 cm $\times$ 30 cm	17 cm $\times$ 8 cm
Stamp Tray Weight	< 500 g	131 g
Speed of Contact	< 1 mm/s	$160 - 320$ µm/s
Resolution of Linear Motion	3.25 µm	0.794 µm.
Maximum Misalignment Handled	In-plane: N/A Out-of-plane: $> 3°$	In-plane: N/A Out-of-plane: $> 3.6°$

This thesis work has:

(i) Designed and fabricated an imprinting device using multiple self-aligning mechanisms in parallel.

(ii) Identified performance metrics that quantify the scalability of the device, including the repeatability of kinematic couplings, parallelism of stages and

fixtures, and parasitics in linear motion. In Chapter 3, these performance metrics were measured and analyzed.

(iii) Developed a model for scalability derived from those performance metrics. As described in Section 2.3.3, the model incorporates angular misalignments at the stamp, slide, and stage level to quantify the maximum number of stamps that can be simultaneously imprinted on the same stage.

(iv) Analyzed the scalability of the DNA imprinting device using the model. In Section 4.1, the scalability model was applied to the device, and it was found that it accommodates stage misalignments of nearly 4°, and stamp and slide misalignments of $> 5°$.

(v) Made recommendations for design improvements and future work, based on the results of the scalability analysis and performance of the device.

While previous work has demonstrated the effectiveness of self-aligning mechanisms in DNA imprinting processes, this thesis work has taken these methods a step further by implementing multiple self-aligning mechanisms in parallel. This work demonstrated a transition from the performance-scale relationship of a 3 degree of motion system, by showing that the reduced complexity of this imprinting device allows achievement of higher performance at larger scales than a 3 degree of freedom system at the same scale.

These efforts will benefit research efforts utilizing nanofluidic transport systems, as the DCI imprinting process provides a low-cost solution to construction of micro/nanowell arrays.[1] By making the process scalable, it becomes more economical for researchers to obtain large quantities of high-quality nanoarrays for protein separation, ion transport, and other biomedical research applications.

5.2 Limitations of Study

In the course of this thesis work, several factors of the DNA imprinting process were left out. These factors, though important in implementation of a fully scalable process, were not crucial to this work's focus on demonstrating the effectiveness of a parallel self-aligning process.

An analysis of stamp force was not undertaken because it was determined to be outside of the scope of this thesis work. However, analysis of the stamp contact force will provide a better understanding of how parasitic motions and frictional forces between the stamp and slide affect the yield of the DCI process. As discussed in Section 1.1.2, high contact forces between the stamp and slide can damage the delicate nanostrands, reducing the yield of the imprinting process and reducing the process's scalability. While this device fulfills its primary purpose of scalably aligning multiple stamps, it remains to be seen whether this alignment scheme reduces defects in the products.

Similarly, although some analysis of parasitic motions during the imprinting process was done, the in-plane orientation of the stamp was not aligned with the slide during the imprinting process. While it will be useful to identify the region of the slide where the stamp is most likely to make contact, it was enough for this thesis work to recognize in general if a stamp would make contact with a slide.

Finally, full automation of the process was not implemented for this work, and the imprinting stage and imprinting process remain largely separate from the other processes. While design components such as the contact switch and interchangeable trays were chosen with automation in mind, the ability of the device to interface with other parts of the DCI process was not a priority. Similarly, although the linear tray design was chosen to enable automated

dispensing along a linear slide, the implementation of a linear dispensing stage was not a focus of this work.

5.3 Potential for Future Work

Based on the limitations and implications of this work, there are several aspects worth examination in more detail:

(i) Contact forces on the stamps. If contact forces are found to be too high, the options to reduce them are limited, and aside from modifying parameters like the actuation speed, additional force control mechanisms would need to be built to mitigate contact force concerns.

(ii) Fixturing of stamps and slides. While in-plane alignment was not a focus of this work, exploration of methods to fixture the stamps and slides could improve the scalability of the process by reducing the potential for misalignments.

(iii) Automation of the system. Ultimately, this device was designed to be part of an entirely automated DCI process. This work has demonstrated the scalability of the parallel self-aligning scheme, and a logical step forward would be incorporation of this device into a fully automated process.

APPENDIX

A

EXPERIMENTAL PROCEDURES

A.1 Kinematic Coupling Repeatability

Since the goal of this experiment is to determine the repeatability of the coupling, the dial gauges will initially be zeroed along the edges of the tray when it is loaded onto the stage in the measurement stage. Subsequent measurements after repeated installation and removal of the tray will yield the movement of the tray from its initial position.

Based off the experiments performed by Slocum, 3 dial gauges were used in the first set of measurements to provide a set of 3 points for analyzing the rotation and translation of the tray.[7] As shown in Figure A.1, the gauges are set up to take measurements at two corners of the tray, with two gauges measuring x-displacement, and the other measuring y-displacement.

The rotation of the tray with respect to its reference position is determined using a dot product. For both the reference position and the measured position, a vector is assumed to run from one measurement point to another. Defining the x-component of the vector as a length l, and the y-component as a height h, the vector notation for the reference vector can be determined using the geometry of the tray alone:

$$\hat{r} = (l, h) \tag{A.1}$$

Taking the experimental measurements into account, the x- and y- components of the measured vector can be found through a similar process:

$$\hat{m} = (l', h') \tag{A.2}$$

Now having two vectors to compare, the definition of a dot product is used to find the angle θ between the reference vector $\hat{r}$ and the measured vector $\hat{m}$:

$$\theta = \cos^{-1}\left(\frac{\hat{r} \cdot \hat{m}}{\|\hat{r}\|\|\hat{m}\|}\right) = \cos^{-1}\left(\frac{l \times l' + h \times h'}{sqrt(l^2 + h^2) \times sqrt(l'^2 + h'^2)}\right) \tag{A.3}$$

This vector method was first applied to the longest vector, as it offered the greatest chance of sufficient resolution.

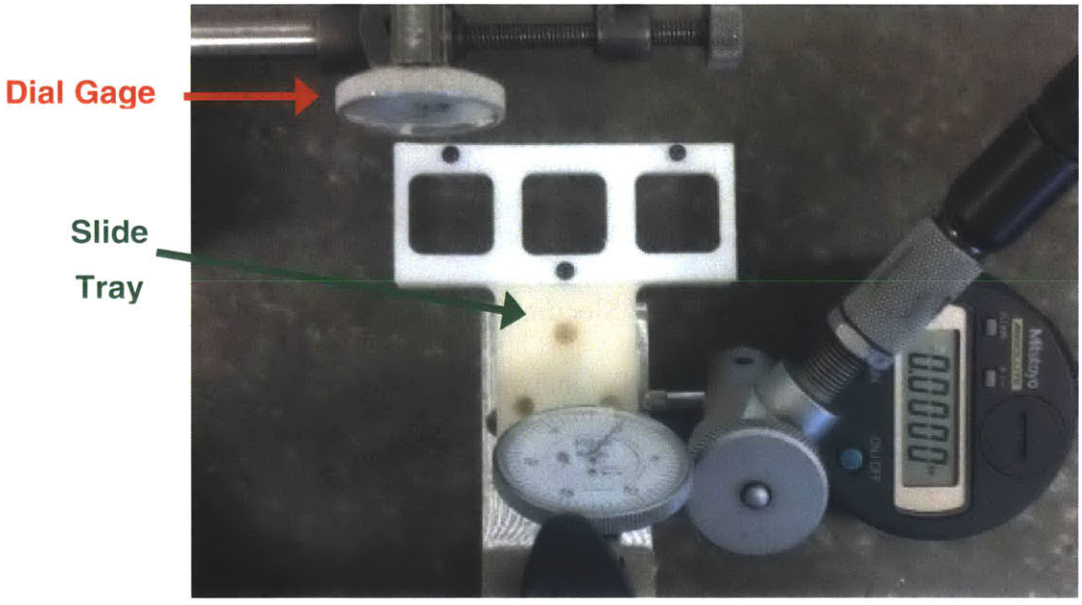

Figure A.1: Experimental setup used to determine kinematic coupling repeatability with respect to in-plane rotation and translation.

To calculate the translation the tray was assumed to rotate around the center of the kinematic coupling. This point was defined as the origin. From this origin, the location of two of the measurement points (one measuring x, and one measuring y) was calculated using part geometry and measurements from the experiment setup. Then, for each of these points, a rotation

matrix was applied using the calculated rotation to obtain predicted values for those same points in the rotated frame:

$$\begin{bmatrix} x' \\ y' \end{bmatrix} = \begin{bmatrix} \cos\theta & -\sin\theta \\ \sin\theta & \cos\theta \end{bmatrix} \begin{bmatrix} x_0 \\ y_0 \end{bmatrix} \tag{A.4}$$

Since each measurement point is only capable of measuring along one axis, it was assumed that the other dimension stayed the same. For a point measuring x-displacement, it was only necessary to calculate x', as it would not register movement in the y-dimension.

The values given by the rotation matrix assume rotation about the center of the kinematic coupling on the stage; that is, they assume no translation, only rotation. By comparing these predicted values to the measured values, the translation of the tray may be determined. If the expected point was the same as the measured point, then the tray had not moved in that direction. If it had, then the distance traveled was the difference between the expected and measured points.

For the second set of measurements, the dial gauges provided a set of 4 points for each measurement. From these 4 points, an equation representing the tilt of the tray can be derived. Figure shows the measurement points and coordinate system used, as well as the axes of rotation. The x and y positions of the measurement points are fixed in space, as the dial gauge only permits measurement along one axis, in this case, the z-axis. The measurement points are then analyzed in pairs, to obtain the rotation about two perpendicular axes.

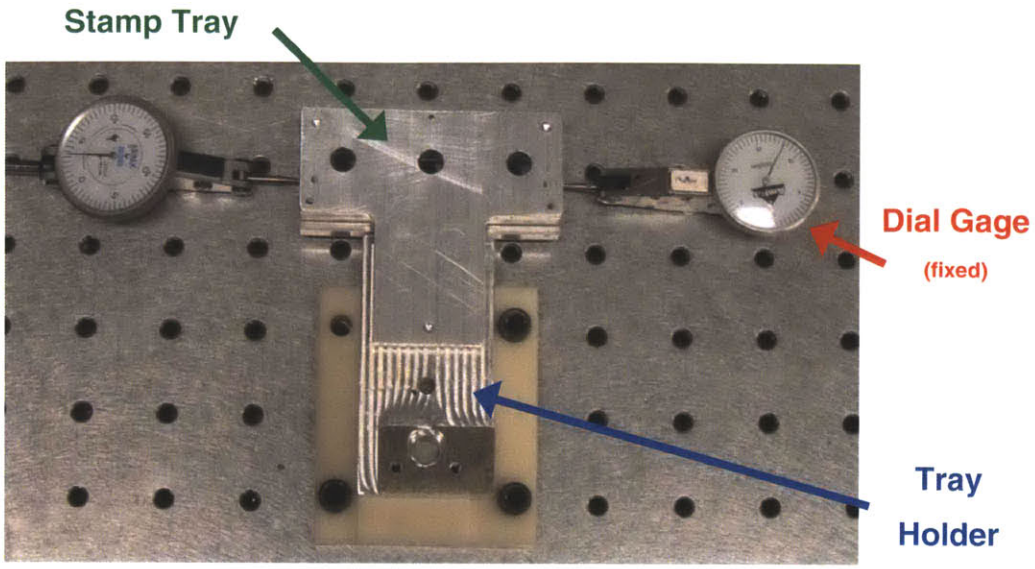

Figure A.2: Experimental setup used to measure the roll of the stamp tray with dial indicators

If the line connecting opposite measurement points is chosen to define an axis of rotation, measurement from the orthogonally oriented gauges can be used to measure the rotation about that axis. For example, the displacement measurements from Points 1 and 2 in Figure can be used to measure rotation about the axis connecting Points 3 and 4. Figure A.3 illustrates this concept.

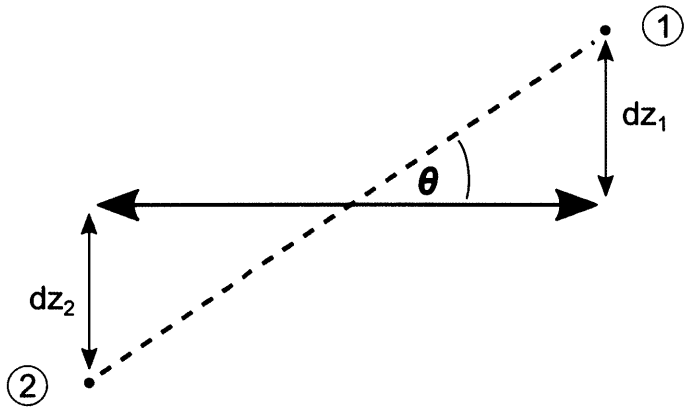

Figure A.3: Diagram depicting the relationship between the measurements taken and the roll angle θ.

From here, the angle of tilt is readily determined using the measurements and the original length between the points:

$$\theta = \tan^{-1}\left(\frac{|z_1 - z_2|}{x_0}\right) \tag{A.5}$$

The roll variation, which which will be called ϕ, was calculated in a similar fashion:

$$\phi = \tan^{-1}\left(\frac{|z_3 - z_4|}{y_0}\right) \tag{A.6}$$

Again, as with the in-plane motion analysis, these measurements were taken by repeated insertion and removal of the trays. The measurement points used were on the bottom surface of the trays, as this enabled the use of calculations mentioned above.

Since the axes for the tilt measurements were defined as the axes of symmetry, determination of the z-translation can be determined by the intercept with the axis of symmetry; if θ and ϕ represent the slopes of the line connecting the measurement points, the z-translation is represented by the intercept.

A.2 Characterization of Linear Motion

The experimental setup and analysis for the linear motion study was very similar to that of the kinematic coupling study. However, this time the stages were loaded into the imprinting device for measurement. As Figure A.4 shows, a set of 3 dial gages was placed around the edge of the stage. As before, these gages were used to measure displacements of the stage, but this time, measurements were taken at the top and bottom positions of imprinting cycles. The point of rotation used for this analysis was the point at the center of the stage against the rail, where it connected to the bearing block.

This method yielded 2 sets of data points: one for when the slide tray was in the open position as it would be for loading, and the other when the slide tray was in the closed position for imprinting and dispensing. Using this data, both the repeatability and the parasitic movements of the linear motion stage were determined.

For both the open and closed positions, the repeatability of the stage's position was calculated as it was for the kinematic couplings. These findings are summarized in Table 3.3, and represent the stage's ability to maintain alignment from cycle to cycle.

For each cycle, the in-plane parasitic motion of the stage was also analyzed. This was accomplished by comparing the measurements for each cycle's open and closed position to find out how much the stage translated or rotated during the transition from its open to closed state.

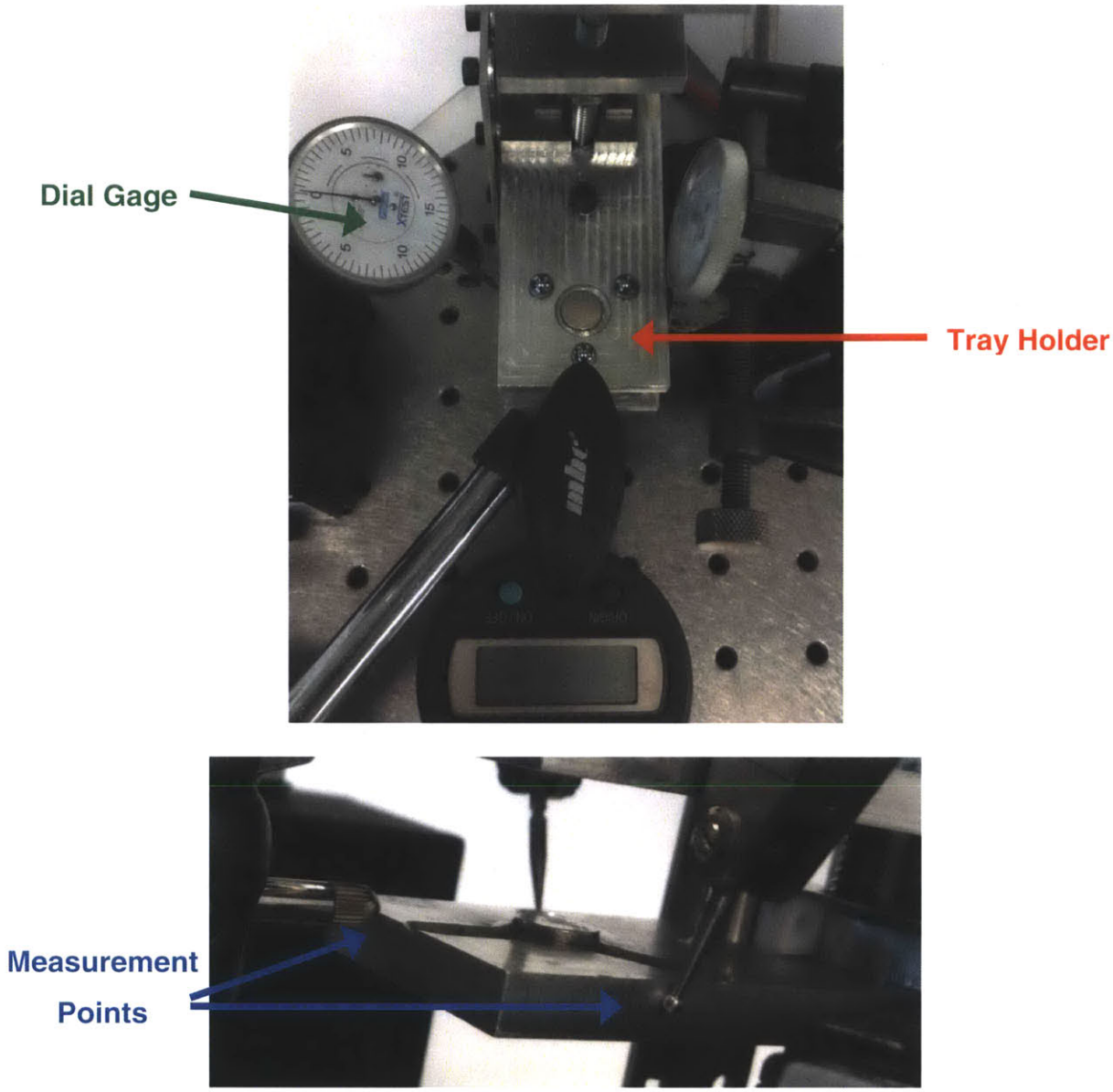

Figure A.4: Experimental setup for characterization of linear motion

REFERENCES

[1] Guan, J. *et al.* "Large laterally ordered nanochannel arrays from DNA combing and imprinting" *Adv. Mater.* **22**, 39997-4001 (2010).

[2] Boukany, P. E. *et al.* "Nanochannel electroporation delivers precise amounts of biomolecules into living cells" *Nature Nanotech* **6**, 747-754 (2011).

[3] Oriental Motor, "PK243-01AA Stepping Motor," accessed May 2012, < http://catalog.orientalmotor.com>

[4] Interinar Electronics, "BSD-013G User Manual," accessed May 2012, < http://www.interinar.com/public_docs/BSD-013G_User_Manual.pdf>

[5] LabVIEW (Version 8.6.1) [Software]. National Instruments, 2008.

[6] Intelitek, "Benchman MX CNC Machining Center," accessed May 2012, <http://www.intelitek.com/admin/Products/uploads/File/File1_9.pdf>

[7] A.H. Slocum, A. Donmez, "Kinematic couplings for precision fixturing — Part 2: Experimental determination of repeatability and stiffness" *Precis. Eng.* **10**, 115-122 (1988).